Title

The 24-kDa subunit of mitochondrial complex I regulates growth, microsclerotia development, stress tolerance, and virulence in Verticillium dahliae.

Journal

Journal of Biology, 22(1)

Authors

Li, Huan

Liu, Ying

Wang, Dan

et al.

Publication Date

2024-12-18

DOI

10.1186/s12915-024-02084-9

Peer reviewed

BMC Biology

RESEARCH

Open Access

The 24-kDa subunit of mitochondrial complex I regulates growth, microsclerotia development, stress tolerance, and virulence in *Verticillium dahliae*

Huan Li[1,2], Ying Liu[1], Dan Wang[4], Ya-Hong Wang[1], Ruo-Cheng Sheng[1,2], Zhi-Qiang Kong[2,3], Steven J. Klosterman[5], Jie-Yin Chen[2,3], Krishna V. Subbarao[6*], Feng-Mao Chen[1*] and Dan-Dan Zhang[2,3*]

Abstract

Background The complete mitochondrial respiratory chain is a precondition for maintaining cellular energy supply, development, and metabolic balance. Due to the evolutionary differentiation of complexes and the semi-autonomy of mitochondria, respiratory chain subunits have become critical targets for crop improvement and fungal control. In fungi, mitochondrial complex I mediates growth and metabolism. However, the role of this complex in the pathogenesis of phytopathogenic fungi is largely unknown.

Results In this study, we identified the NADH: ubiquinone oxidoreductase 24-kDa subunit (VdNuo1) of complex in vascular wilt pathogen, *Verticillium dahliae*, and examined its functional conservation in phytopathogenic fungi. Based on the treatments with respiratory chain inhibitors, the mitochondria-localized VdNuo1 was confirmed to regulate mitochondrial morphogenesis and homeostasis. VdNuo1 was induced during the different developmental stages in *V. dahliae*, including hyphal growth, conidiation, and melanized microsclerotia development. The *VdNuo1* mutants displayed variable sensitivity to stress factors and decreased pathogenicity in multiple hosts, indicating that VdNuo1 is necessary in stress tolerance and full virulence. Comparative transcriptome analysis demonstrated that VdNuo1 mediates global transcriptional effects, including oxidation and reduction processes, fatty acid, sugar, and energy metabolism. These defects are partly attributed to impairments of mitochondrial morphological integrity, complex assembly, and related functions. Its homologue (*CgNuo1*) functions in the vegetative growth, melanin biosynthesis, and pathogenicity of *Colletotrichum gloeosporioides*; however, *CgNuo1* does not restore the *VdNuo1* mutant to normal phenotypes.

Conclusions Our results revealed that *VdNuo1* plays important roles in growth, metabolism, microsclerotia development, stress tolerance, and virulence of *V. dahliae*, sharing novel insight into the function of complex I and a potential fungicide target for pathogenic fungi.

*Correspondence:
Krishna V. Subbarao
kvsubbarao@ucdavis.edu
Feng-Mao Chen
cfengmao@njfu.edu.cn
Dan-Dan Zhang
zhangdandan@caas.cn
Full list of author information is available at the end of the article

Keywords *Verticillium dahliae*, NADH: ubiquinone oxidoreductase, Microsclerotia development, Stress tolerance, Pathogenicity

Background

Mitochondria are well known for their role as cellular powerhouses, providing adenosine triphosphate (ATP), the primary energy currency. In eukaryotes, these double membrane-bound organelles perform various functions such as the oxidative metabolism, maintenance of cellular calcium and iron homeostasis, degradation of toxins, and feedback on integrated stress responses, as well as mitochondrial-to-nuclear communication [1–4]. Furthermore, the intermediaries of mitochondrial metabolism promote epigenetic modification [5] and participate in the biosynthesis of heme and amino acids [6]. Among these, components of oxidative phosphorylation have become a focus for mitochondrial research due to their importance in mitochondrial origin hypothesis, disease occurrence, microbial stress tolerance, host–pathogen interactions, and as targets for the innovation of new fungicides [7, 8].

The oxidative phosphorylation that occurs in the mitochondrial electron transport chain (ETC) comprises five inner mitochondrial membrane (IMM)-embedded enzymatic complexes (complex I, II, III, IV, and V) and two mobile electron carriers (ubiquinone and cytochrome c) [9, 10]. Functionally, the ETC utilizes the changes in the oxidation and reduction states of substrates to establish electron flow coupled with the accumulation of a proton electrochemical gradient across the IMM to produce ATP [3, 9, 11, 12]. Besides electron transport, the ETC also generates metabolites tightly associated with redox homeostasis, aging, signal transduction, and other physiological and biological functions [5, 13]. For example, a byproduct of oxidative phosphorylation, NAD^+, is crucial in inducing mitochondrial development and autophagy [14]. The mitochondrial reactive oxygen species (mtROS) trigger mitochondrial membrane depolarization and act as a signal to mediate mitochondria-nuclear communication [5, 15].

Mitochondria are recognized to have evolved from endosymbiotic α-proteobacteria. Thus, as one of the semi-autonomous organelles, they independently regulate the coding of 13 ETC subunits (complex I, III, IV, and V contain 7, 1, 3, and 2 subunits, respectively) [16–18], and thus collaboration with the nucleus is important for complex assembly and ultimately ATP synthesis. Complex I is the largest respiratory chain unit with 45, 49, and 42 subunits in mammals, plants, and yeast, respectively [3, 10, 19]. Although about 30 components of complex I are evolutionarily independent, its 14 core subunits are highly conserved in mammals, plants, yeast, and bacteria [20]. Based on hydrophilic and hydrophobic characteristics, the 14 core subunits distributed on the peripheral and membrane arms of complex I are divided into N, Q, and P modules of 3, 4, and 7 core subunits, respectively [3, 18]. The P module is embedded in the membrane arm of the IMM connected with peripheral arm by the Q module, while the tip N module of the peripheral arm is immersed in the mitochondrial matrix. These modules form an L-like membrane-spanning skeleton and function in proton pumping, quinone reduction, and NADH oxidation, respectively [9, 21, 22]. Notably, the effects of mis-assembly and damage of complex I on cells are global. In humans, complex I dysfunction or loss causes 20 ~ 30% of mitochondrial diseases, such as Leigh syndrome, Parkinson's disease, lactic acidosis, neuropathy, and myopathy [23, 24]. Complex I is involved in plant development and seed maturation, and its function in mtROS metabolism confers plant resistance to biotic and abiotic stresses [18, 25].

In fungi, complex I mediates vegetative growth, stress tolerance, metabolism, and virulence. The defects of subunit Ndi1p resulted in the abolishment of sporulation in yeast [26]. Citrinin and pigment biosynthesis are negatively correlated with complex I activity in *Monascus purpureus* [27]. The subunit Nuo2 of complex I in *Candida albicans* regulates commensalism and plays a vital role in carbon source utilization, hyphal growth, biofilm formation, and virulence [28]. The mtROS, and especially superoxide anions produced by electron leakage of complex I, can attack the IMM and induce mitochondrial autophagy [29]. Moreover, the two subunits, NDE1 and NDE2, have been found to cooperatively maintain mtROS by regulating catalase activity [30]. Furthermore, due to evolutionary differences of complex I among mammals, plants, and fungi, complex I is also a novel fungicide target. For example, the mono-alkyl lipophilic cations (MALCs) fungicide C_{18}-SMe_2^+ inhibits oxidative phosphorylation by reducing NADH oxidation and depolarizing the IMM and induces mtROS accumulation to trigger fungal apoptosis [8]. Mitochondrial inheritance and its functions in homeostasis are essential for virulence of fungal pathogens [31, 32]; however, the role of complex I in homology, growth, stress resistance, and pathogenicity of plant pathogenic fungi remains obscure.

Verticillium dahliae is a notorious soil-borne phytopathogenic fungus in the genus *Verticillium*. It causes

destructive Verticillium wilt in more than 200 dicotyledon plants, including a variety of economically important crops and trees [33–35]. *V. dahliae* is difficult to control, owing to the melanized dormant microsclerotia with long-term vitality and adaptability in soil [36, 37]. The microsclerotia give rise to hyphae that invade the plant through the roots and proliferate upward through xylem vessels. During this process, various secreted effectors and toxic metabolites of *V. dahliae* and defense responses of the plant contribute to vascular clogging and wilt [38]. Infected plants exhibit developmental retardation, leaf yellowing and wilting, vascular tissue discoloration, and even death [34, 39]. Studies in *V. dahliae* focusing on secondary metabolism, signaling pathways, posttranslational modifications, transcriptional regulation, and effector protein activities have revealed the roles of these processes in growth, host adaptability, melanized microsclerotia development, stress resistance, and pathogenicity [38, 40–44]. Some evidence indicates that the disturbance of mitochondrial ATP output and mtROS metabolism inhibits growth and virulence and induces apoptotic cell death in *V. dahliae* [45, 46]. Differences in virulence between strains of *V. nonalfalfae*, with a mitochondrial genome closely related to *V. dahliae*, have also been attributed to both nuclear and mitochondrial genomes of the causal strains [16]. Hence, the functional analysis of complex I subunits is a valuable undertaking to elucidate developmental characteristics and pathogenesis of *V. dahliae*.

In this study, the NADH: ubiquinone oxidoreductase 24-kDa subunit (VdNuo1) of complex I in *V. dahliae* was demonstrated to mediate vegetative growth, melanin biosynthesis, microsclerotia development, stress tolerance, and pathogenicity. Further, comparison of the transcriptional profiles of the *VdNuo1* mutant and the wild-type strain provided global views of the role of *VdNuo1* in metabolism, oxidation–reduction, transcriptional regulation, and mitochondrial function of *V. dahliae*. The contribution of VdNuo1 to the integrity of mitochondrial membrane system was also determined by transmission electron microscopy. Taken together, our results revealed pleiotropic functions of the core subunit VdNuo1 in *V. dahliae*. Analyses of the homology between VdNuo1 and its orthologs suggested that although Nuo1 functions are conserved in development and pathogenicity of *Colletotrichum gloeosporioides*, CgNuo1 is incompatible in *V. dahliae*.

Results

Mitochondrion-localized NADH: ubiquinone oxidoreductase 24-kDa subunit (VdNuo1) is conserved in filamentous fungi

In our previous study, a genomic sequence fragment encoding 10 homologues was identified as conserved in *V. dahliae* and *C. gloeosporioides* [43]. Among these homologues, two zinc finger proteins, VdZFP1 and VdZFP2, were confirmed to positively regulate the hyphal growth, melanin biosynthesis, and microsclerotia development of *V. dahliae* by interacting with VdCmr1 [43]. Notably, the NADH: ubiquinone oxidoreductase 24-kDa subunit coding gene named *VdNuo1* (*DK185_04253* in AT13 (https://db.cngb.org/Verticilli-Omics/); *VDAG_08642* in VdLs.17 [33]) is adjacent to the VdZFPs. As the core subunit of complex I, the exact function of NADH: ubiquinone oxidoreductase 24-kDa subunit is largely unknown in plant pathogenic fungi.

To determine whether VdNuo1 is a component of the mitochondrion where it may function in the respiratory chain, we initially examined its subcellular localization. The plasmid containing green fluorescent protein (GFP) fused with VdNuo1 was transformed into the WT *V. dahliae* strain AT13. As predicted, the GFP signal of the VdNuo1-eGFP fusion strain (WT-VdNuo1::eGFP) was co-localized with the red fluorescence of the mitochondrial probe CMXRos (Fig. 1A). The intensity of green and red fluorescence was also consistent (Fig. 1C). These results indicated that VdNuo1 is localized in mitochondria. In contrast, the GFP signal of eGFP-integrated strain (WT-eGFP) was present in the cytoplasm (Fig. 1A and B).

Subsequently, the sequence information and three-dimensional structure of VdNuo1 were predicted by the SMART, InterPro, MitoFates, and SWISS-MODEL online tools. VdNuo1 encodes 265 aa (amino acids), and possesses a conserved mitochondrial presequence (N-terminal 23 aa, Fig. 1D) and a TRX-like [2Fe-2S] ferredoxin family domain (from 130 to 211 aa, Fig. 1D) that facilitates electron transfer [9]. Spatial models indicate that residues 136C, 141C, 179C, and 183C in VdNuo1 are involved in binding of iron-sulfur (FeS) clusters (Fig. 1E). Phylogenetic analysis showed that VdNuo1 shared the closest evolutionary relationship within *Verticillium* spp., while the clustering result revealed that VdNuo1 and its homologues in filamentous fungi were evolutionarily conserved and shared the same ancestral origin (Fig. 1F).

VdNuo1 is crucial for respiratory chain homeostasis and metabolism

To investigate the physiological and biological functions of VdNuo1, *VdNuo1* deletion mutants (Δ*VdNuo1*) and ectopic complemented transformants ($EC^{\Delta VdNuo1}$) were obtained by homologous recombination and reintroduction of *VdNuo1* into the deletion mutants, respectively. All mutants were verified by multiple diagnostic PCR assays (Fig. S1A–C).

Given the importance of the 24-kDa subunit in complex I enzyme activity [47], three respiratory chain inhibitors of complex I, II, and III were introduced to

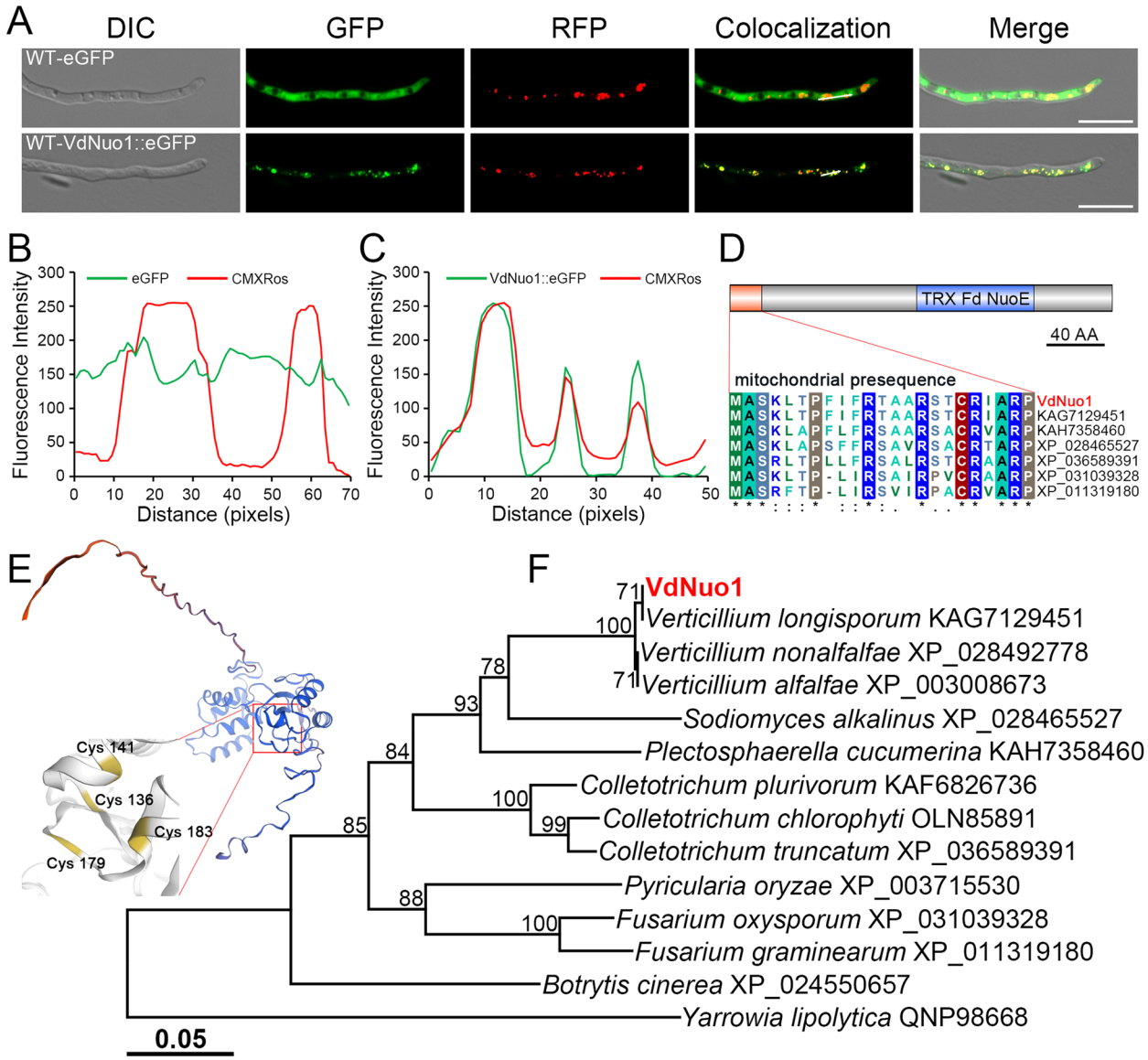

Fig. 1 The mitochondria-localized VdNuo1 from *Verticillium dahliae* is conserved in filamentous fungi. **A** Subcellular localization of VdNuo1 in *V. dahliae*. A VdNuo1-GFP fusion was introduced into the WT strain AT13, and the positive transformants were incubated on hydrophobic glass slides in the dark at 25 °C for 16 h. Before observation, the germinating hyphae of the WT, VdNuo1 mutants, and complemented strains were stained using the mitochondrial probe (CMXRos). The GFP and RFP signals were observed by fluorescence microscopy. Scale bar = 10 μm. **B** and **C** Fluorescence intensity analysis of GFP and RFP signals in **A**. The co-located images were split into GFP and RFP channels, and the signal strength was obtained by ImageJ software. **D** Domains within the protein sequence of VdNuo1 were predicted by multiple pipelines of MitoFates, SMART, InterPro, and Pfam. The FeS cluster, NuoE motif, and putative mitochondrial presequence were labeled by IBS software (Illustrator for Biological Sequences). Scale bar = 40 amino acids. **E** Three-dimensional structure prediction of VdNuo1. The spatial structure and core cysteine residues were analyzed using SWISS-MODEL. **F** Phylogenetic analysis of VdNuo1 from *V. dahliae* and its homologues from other fungi. The protein sequences were downloaded from the National Center for Biotechnology Information database (https://www.ncbi.nlm.nih.gov/). The phylogenetic tree was constructed using MEGA 7.0 with neighbor-joining algorithm. The branch nodes were evaluated using 1000 bootstrap replications

assess the effects of *Vdnuo1* deletion on the mitochondrial ETC in *V. dahliae*. Rotenone and dimercaprol specifically block the electron transfer process from FeS centers to ubiquinone and from QH2 to cytochrome c, respectively, whereas carboxin inhibits activity of succinate dehydrogenase [7, 48, 49]. The WT, Δ*VdNuo1*, and *VdNuo1* complemented strains were inoculated on Czapek-Dox agar (Czapek) medium supplemented with the three inhibitors independently for analyses of respiratory chain tolerance. Compared with the WT

and complemented strains, *VdNuo1*-deletion mutants showed different sensitivities to inhibitors. Deletion of *VdNuo1* resulted in significant tolerance of *V. dahliae* to both complex I and II inhibitors, but greater sensitivity to dimercaprol (Fig. 2A). The levels of growth inhibition of *VdNuo1* mutants on 12 μM rotenone and 20 μM carboxin plates were nearly half that of WT strain, while growth of 100 μM dimercaprol-treated mutants increased by 60% (Fig. 2B). Complementation of *VdNuo1* restored these defects (Fig. 2A and B). These results suggested that *VdNuo1* is essential to maintain mitochondrial respiratory chain homeostasis in *V. dahliae*.

Fungal sugar and fatty acid metabolism are mainly dependent on mitochondrial activity [27]. Sugar and fatty acid utilization of each strain was examined. To eliminate the influence of various sugars on the growth of the WT strain, we examined the diameter ratio of *VdNuo1* mutants to WT to evaluate the role of VdNuo1 in sugar metabolism. The ratios illustrated that *VdNuo1* is important for sugar metabolism in *V. dahliae* (Fig. S2A and B). Fatty acids are required for fungal development, energy supply, and virulence. However, excess fatty acids are harmful to fungi [50, 51]. Colony phenotypes and inhibition rates showed that the *VdNuo1* deletion mutants were more sensitive (increase inhibition rate by approximately 40%) to linoleic acid and linolenic acid than the WT and complementary strains (Fig. S2C and D). Quantitative analysis of fatty acids also confirmed that the deletion of *VdNuo1* significantly reduced (about 90%) the fatty acid content (Fig. S2E). More importantly, the metabolic balance of unsaturated fatty acids in *VdNuo1* mutants was disturbed. About 30% of monounsaturated fatty acids were replaced by polyunsaturated fatty acids (Fig. S2F).

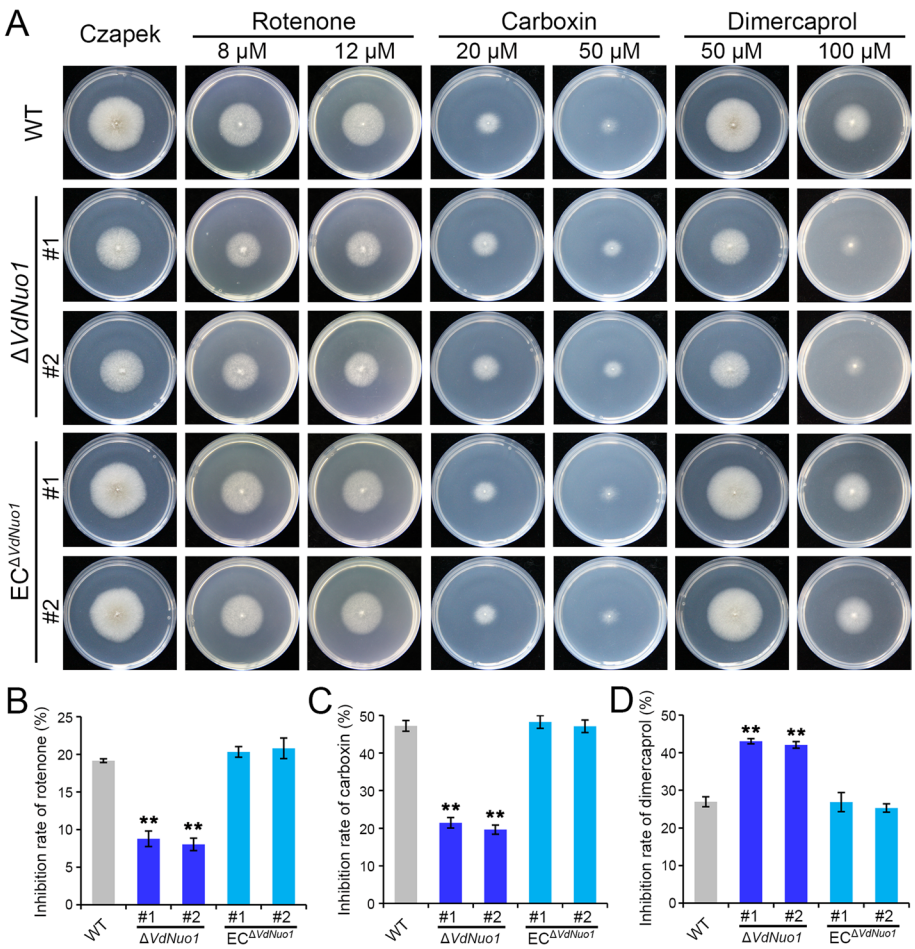

Fig. 2 *VdNuo1* functions in the mitochondrial respiratory chain of *Verticillium dahliae*. **A** The response of WT, *VdNuo1* mutants, and complemented strains to mitochondrial complex I, II, and III inhibitors. The colony morphology of WT, *VdNuo1* mutants, and complemented strains grown on Czapek medium were supplemented with different concentrations of inhibitors at 25 °C in the dark. Each strain was inoculated on at least three plates and three independent experiments were carried out. **B**, **C**, and **D** The inhibition rates of inhibitors. Colony diameter of indicated strains on medium with 8 μM rotenone, 20 μM carboxin, and 100 μM dimercaprol. Error bars are standard errors calculated from six plates, and this experiment was replicated three times. $^{*}P < 0.05$, $^{**}P < 0.01$ (Student's *t*-test)

These results indicated that *VdNuo1* is important for metabolism of fatty acids and sugars in *V. dahliae*.

VdNuo1 is involved in *V. dahliae* growth, conidiation, and development

To determine the role of *VdNuo1* in *V. dahliae* growth, WT, Δ*VdNuo1*, and EC$^{\Delta VdNuo1}$ strains were cultured on potato dextrose agar (PDA), Czapek, and different carbon source media for 7 days. Consistent with sugar utilization phenotypes, deletion of *VdNuo1* severely impaired the radial growth of *V. dahliae* (Fig. 3A–C). Starch, pectin, and sodium carboxymethyl cellulose (CMC-Na) were used to simulate host components of *V. dahliae*. Growth retardation on each carbon source (Fig. 3A and D–F)

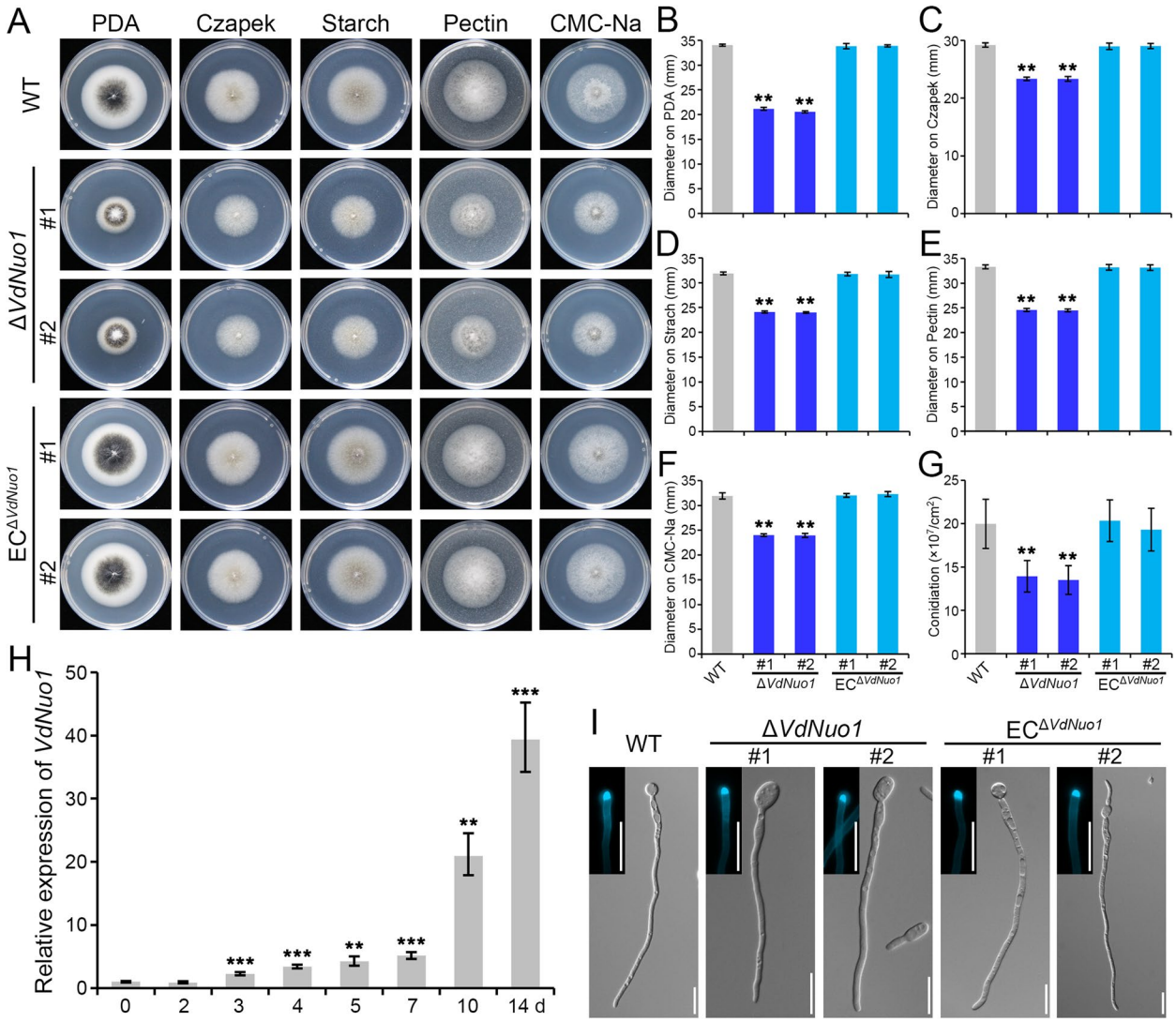

Fig. 3 *Vdnuo1* mediates vegetative growth in *Verticillium dahliae*. **A** The colony phenotypes of WT, *VdNuo1* mutants, and complemented strains in response to different carbon sources. All strains were cultured on PDA and Czapek salt medium containing either sucrose, starch, pectin, or sodium carboxymethyl cellulose (CMC-Na) at 25 °C in the dark for 7 days. Each strain was inoculated on at least three plates and three independent experiments were carried out. **B**, **C**, **D**, **E**, and **F** The colony diameter of the indicated strains in **A**. Error bars are standard errors calculated from six plates, and this experiment was replicated three times. $^{*}P < 0.05$, $^{**}P < 0.01$ (Student's *t*-test). **H** Relative expression of *VdNuo1* in WT life cycle cultured in the laboratory. The strains were cultured on BMM medium at 25 °C in the dark. The RNA samples were collected at 2, 3, 4, 5, 7, 10, and 14 dpi. RT-qPCR detection was independently repeated three times with 0 dpi (conidia) as control, and the results were conducted using the $2^{-\Delta\Delta CT}$ method. Error bars represent standard errors of the mean, $^{**}P < 0.01$, and $^{***}P < 0.001$ (one-way ANOVA). **I** Hyphal morphology of WT, *VdNuo1* mutants, and the complemented strains. The conidial suspensions of all strains were incubated on hydrophobic glass slides in a dark at 25 °C for 16 h. CFW was used to stain the chitin of each strain. The germinating hyphae and distribution of chitin were observed by fluorescence microscopy. Scale bar = 10 μm

further confirmed the importance of *VdNuo1*-mediated vegetative growth. Meanwhile, the number of conidia of each strain cultured on PDA medium suggested that deletion of *VdNuo1* can significantly compromise the conidiation of *V. dahliae* (Fig. 3G). The colony diameter and conidiation of the complemented strains were similar to that of the WT strain.

The developmental phases in the growth cycle of *V. dahliae* include hyphal growth, production of conidia, microsclerotia precursor formation, and microsclerotia maturation [41]. To explore whether *VdNuo1* is involved in these developmental phases, we analyzed the gene expression profile in *V. dahliae* incubated on modified basal agar medium (BMM) from 0 to 14 dpi (day post inoculation). The persistent upregulation of expression levels of *VdNuo1* (Fig. 3H) suggested that *VdNuo1* is important for development and even dormancy of *V. dahliae*. A decrease in the diameter of the Δ*VdNuo1* strain was observed, likely due to polar growth defects. To examine the potential effect of VdNuo1 on polar growth, the conidia of each strain were incubated on hydrophobic glass slides for 12 h. The germinating hyphae were stained with Calcofluor White (CFW) and observed by fluorescence microscopy. The normal hyphal morphology and chitin distribution at the hyphal apex among WT, deletion mutants, and complemented strains suggested that deletion of *VdNuo1* did not impair polar growth (Fig. 3I). Overall, these results indicated that *VdNuo1* participates in growth, conidiation, and development of *V. dahliae*.

VdNuo1 mediates development and melanization of microsclerotia

Microsclerotia are melanized survival structures and the primary inoculum of *V. dahliae* [34, 37]. Melanin was observed in mutants (Fig. 3A), and the expression profile indicated that the expression of *VdNuo1* is induced during microsclerotia maturation (Fig. 3H). To examine this further, the WT, Δ*VdNuo1*, and $EC^{\Delta VdNuo1}$ strains were incubated on BMM medium and the formation and maturation of microsclerotia were observed regularly with a stereoscopic microscope. At 5 dpi, the WT and complemented strains formed swollen and moniliform microsclerotia precursors accompanied by melanin deposition (Fig. 4A). However, the hyphae of *VdNuo1* mutants were transparent and relatively smooth (Fig. 4A). The mature microsclerotia of WT and complemented strains continued forming until 7 days, but only limited precursors accumulated melanin in *VdNuo1* deletion mutants on BMM medium (Fig. S3). Although mature microsclerotia formed in all strains at 14 dpi, their density, size, and melanization were different between strains (Fig. 4A). Specifically, compared with the WT and complemented strains, more (~50% increase) and smaller (~40% reduction in volume) microsclerotia formed in *VdNuo1* mutants, also exhibiting melanin deposition defects (reduce ~50%) (Fig. 4B–D). Microsclerotia melanization is accompanied by the strong expression of melanin biosynthesis genes [52]. Remarkably, only the genes of the melanin pathway, but not upstream regulators (*VdZFP1* and *VdZFP2*), were suppressed in the *VdNuo1* mutant, and mutant complementation rescued these defects (Fig. 4E). Together, these results suggested that *VdNuo1* acts as a positive regulator of microsclerotia development and melanin biosynthesis in *V. dahliae*.

Previous studies confirmed that VdSho1 contributes to the formation of penetration pegs in hyphopodia and also positively regulates melanin biosynthesis [53]. Thus, given the correlation between melanin accumulation and invasive hyphae formation, *VdNuo1* was examined for its potential role in initial colonization of *V. dahliae*. The WT, *VdNuo1* mutants, and complemented strains were inoculated on MM (minimal) medium covered with a cellophane membrane to simulate penetration of the host epidermis. After 3 days of incubation, all strains displayed a similar ability to penetrate the cellophane membrane (Fig. 4F). These results suggested that *VdNuo1*-mediated melanin accumulation is associated with microsclerotia development rather than penetration in *V. dahliae*.

VdNuo1 participates in abiotic stress tolerance and pathogenicity

Melanins confer various functions in fungi and are involved in maintaining homeostasis, development of resistant survival structures, adaptation to environmental cues, niche competition, and host infection [43, 54]. In *V. dahliae*, melanin is mainly deposited at the cell wall of microsclerotial cells to ensure their survival in extreme environments, but its production is not required for pathogenicity [36]. To explore the environmental abiotic stress response of *VdNuo1*, the WT, *VdNuo1* mutants, and the complemented strains were cultured on the PDA medium supplemented with 1.2 M sorbitol, 0.8 M NaCl, 1 M KCl, 0.4 M $CaCl_2$, 0.02% SDS (sodium dodecyl sulfate), and 200 μg/mL CR (congo red) for 7 days, respectively. The inhibition rate showed that *VdNuo1* mutants was more sensitive to cell membrane permeability (NaCl, KCl, and $CaCl_2$) and cell wall integrity (SDS and CR) stresses than the WT and complemented strains, whereas these were more tolerant to osmotic pressure (sorbitol) (Fig. 5A–G). This suggested that *VdNuo1* is necessary for *V. dahliae* to resist abiotic stresses.

To evaluate the contribution of *VdNuo1* to virulence, seedlings of susceptible shantung maple and cotton were inoculated with conidial suspensions of WT, *VdNuo1* mutants, and the complemented strains. The 1-month-old

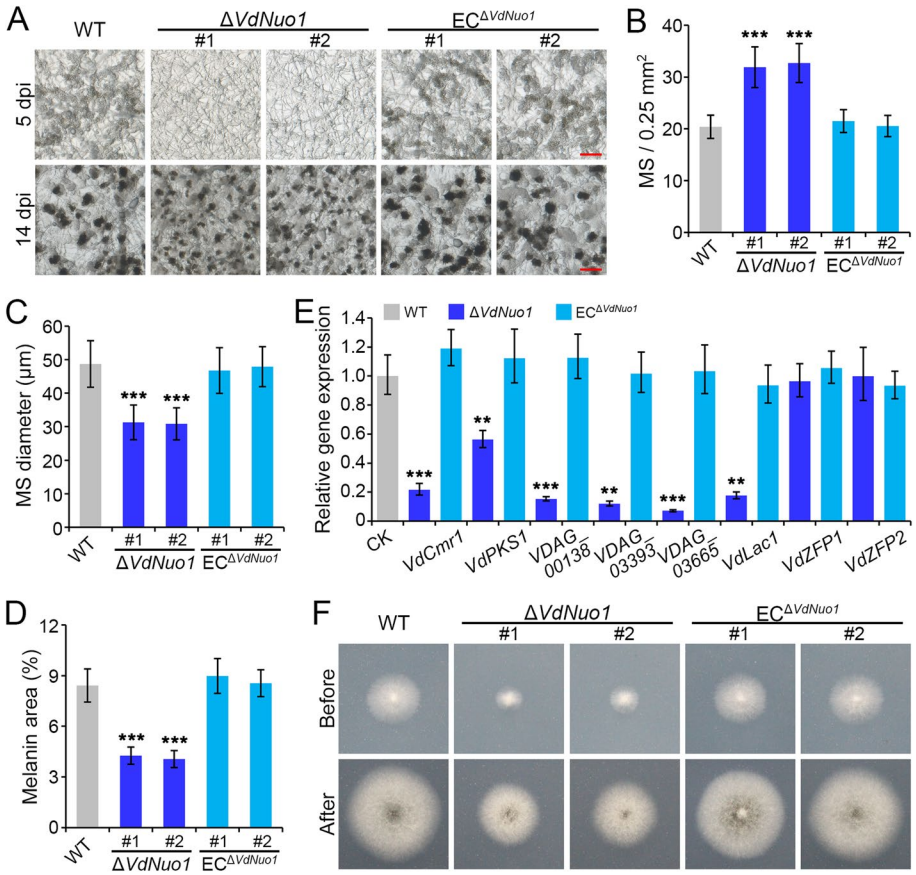

Fig. 4 *VdNuo1* mediates melanin biosynthesis and microsclerotia development in *Verticillium dahliae*. **A** Microsclerotia morphology of WT, *VdNuo1* mutants, and complemented strains. Each strain was cultured on the BMM medium covered with cellophane membranes. The development of microsclerotia was observed at 5 and 14 dpi after incubation at 25 °C in the dark with a stereoscope. This experiment was repeated three times independently. Scale bar = 100 μm. **B**, **C**, and **D** Analysis of differences in the number, size, and melanin coverage of microsclerotia between WT, *VdNuo1* mutants, and complemented strains. All strains were cultured on BMM medium at 25 °C in the dark. After incubating for 14 days, the diameter of 150 mature microsclerotia of each strain were measured, while the number or melanin coverage of microsclerotia was calculated from 60 or 30 visual fields, respectively. **B** microsclerotia number, **C** microsclerotia diameter, and **D** melanin coverage of microsclerotia. Error bars represent the standard deviation of each independent experiment, and all experiments were performed with three replicates, $^{***}P < 0.001$ (Student's *t*-test). **E** Analyses of the relative expression of melanin-related genes during the microsclerotia development among WT, *VdNuo1* mutants, and complement strains. All strains were inducted on BMM medium at 25 °C in the dark and collected at 7 dpi. Compared with WT strain, the expression level of each gene in *VdNuo1* mutants and complement strains was detected by RT-qPCR for 3 repetitions using the $2^{-\Delta\Delta CT}$ method. Quantitative detection was repeated three times, $^{**}P < 0.01$, $^{***}P < 0.001$ (one-way ANOVA). **F** The penetration ability of WT, *VdNuo1* mutants, and complemented strains. The hyphal blocks were inoculated on MM medium covered with cellophane membranes at 25 °C in the dark. The cellophane membranes were removed at 3 dpi. All strains continued to grow for an additional 5 days. This experiment performed with three replicate experiments with six plates per experiment

shantung maple seedlings first exhibited Verticillium wilt symptoms on the 14th day after inoculation with the WT and complemented strains. At 30 to 35 dpi, all plants inoculated with the WT and complemented strains showed defoliation, wilting, and death (Fig. 5H). In contrast, the plants inoculated with the *VdNuo1* mutant strains were healthy, but displayed a slight reduction in height (Fig. 5H). Since the pathogen could not be re-isolated and there was low fungal biomass in stems, this suggested that the deletion of *VdNuo1* reduced the ability of the fungus to proliferate in the infected maple plants (Fig. 5I). Similarly, at 21 dpi, more than 85% of the infected cotton seedlings exhibited foliar wilting, defoliation, vascular discoloration, and even death (Fig. S4A). Until 21 dpi, the seedlings inoculated with *VdNuo1* mutants showed only mild foliar yellowing (Fig. S4A). In addition, the pathogen biomass of *VdNuo1* mutants on cotton was much lower than that of the WT and complemented strains (Fig. S4B). These results suggested that *VdNuo1* is a critically important for the pathogenicity of *V. dahliae*.

Nuo1 homologue is functionally conserved in *C. gloeosporioides*

The proximity in genetic distance (Fig. 1F) indicated that the homologues of *Nuo1* may share conserved functions in *V. dahliae* and *C. gloeosporioides*. To determine if the *VdNuo1* homologue is functional in *C. gloeosporioides*, we initially obtained the deletion mutants (Δ*CgNuo1*) and complementary strains ($EC^{\Delta CgNuo1}$) (Fig. S5A and B). As expected, deletion of *CgNuo1* inhibited the radial growth of *C. gloeosporioides* (Fig. 6A and B). The conidia of each strain were collected and incubated for observations of appressoria, which is accompanied by melanin deposition in *C. gloeosporioides* to produce functional penetration pegs [55]. Compared with the WT strain, the *CgNuo1* mutants formed significantly fewer melanized appressoria, which were replaced with more hyaline appressoria (Fig. 6A and C). Additionally, each strain was inoculated on *Liriodendron chinensis*×*tulipifera* leaves, revealing that the deletion of *CgNuo1* severely compromised the lesion expansion (Fig. 6D and E). The complemented strains restored all these defects (Fig. 6A–E). Taken together, these results confirm that *CgNuo1* is crucial for growth, appressoria melanization, and pathogenicity of *C. gloeosporioides*.

To explore the interspecies compatibility and subcellular localization of *CgNuo1*, we fused *CgNuo1* with GFP fragments in an overexpression plasmid. The recombinant plasmid was transferred to the *VdNuo1* mutant, and the positive transformants were identified by diagnostic PCR (Fig. S5C). The heterologous complemented strains ($\Delta VdNuo1\_OE^{CgNuo1-GFP}$) not only failed to recover colony morphology, but also inhibited the growth of *VdNuo1* mutants (Figs. 6F and S5B). The fluorescent signals of GFP-tagged CgNuo1 co-localized with the red fluorescence of the mitochondrial probe (Fig. 6G), indicating that CgNuo1 was also localized in mitochondria of *VdNuo1* mutant. We thus concluded that the functions of *VdNuo1* homologues are conserved in filamentous fungi, but may be incompatible across species.

Comparative transcriptome analysis reveals *VdNuo1*-mediated mitochondrial functions in *V. dahliae*

To reveal the potential mechanism of the effects mediated by *VdNuo1* on development, metabolism, and virulence, a comparative transcriptome analysis was carried out. The raw data of RNA sequencing (RNA-seq) was filtered and subsequently mapped to the reference genome. In total, compared with the WT, deletion of *VdNuo1* resulted in 2904 (about a third of total genes of *V. dahliae*) differentially expressed genes (fold change ≥ 2.0, $P < 0.01$, 1480 DEGs upregulated) (supplementary Table S4). Gene ontology (GO) enrichment analysis showed that the DEGs were involved in several functional types, such as transcriptional regulation (GO:0005506, GO:0008270, GO:0003700, and others), oxidation–reduction process (GO:0016491, GO:0055114, GO:0020037, and others), oxidative stress (GO:0004096, GO:0004601, GO:0015035, and others), energy metabolism (GO:0005975, GO:0006629, GO:0006807, and others), and mitochondria-related process (GO:0005743, GO:0005759, GO:0005758, and others) (Fig. 7A and B; supplementary Table S4). Meanwhile, Kyoto Encyclopedia of Genes and Genomes (KEGG) pathway analysis suggested that the deletion of *VdNuo1* disrupts a variety of biological processes, including energy metabolism (lipid, fatty acid, carbohydrate, and amino acid), secondary metabolism, aging, and signaling pathways (Fig. 7C; supplementary Table S4). Hence, the terms associated with these DEGs are naturally correlated with morphological development and other biological processes mentioned above. Further, mitochondria-related genes, especially those related to mitochondrial respiratory chain, were overrepresented. Notably, mitochondria-related genes encoding complex subunits, assembly components, electron transfer carriers, cytochrome C oxidase, and others were abundant in DEGs (Fig. 7D and Fig. S6A; supplementary Table S4). These results were consistent with the hypothesis that *VdNuo1* is essential for mitochondrial function.

(See figure on next page.)

Fig. 5 *VdNuo1* contributes to stress response and pathogenicity of *Verticillium dahliae*. **A** Colony morphology of WT, *VdNuo1* mutants, and complemented strains grown on medium supplemented with abiotic stressors. The strains were cultured on PDA medium supplemented with 1.2 M sorbitol, 0.8 M NaCl, 1 M KCl, 0.4 M $CaCl_2$, 0.02% SDS, and 200 μg/mL CR at 25 °C in the dark for 7 days. Each strain was inoculated on at least 3 plates and the experiment was replicated three times. **B–G** Sensitivity of the indicated strains to stress factors (sorbitol, NaCl, KCl, $CaCl_2$, SDS, and CR, respectively). The inhibition rate of above strains responsible for various stressors in **A** was calculated upon colony diameter. Error bars are standard errors calculated from six replicates with PDA plates as controls, and this experiment was replicated three times. $^{*}P < 0.05$, $^{**}P < 0.01$, $^{***}P < 0.001$ are probabilities associated with the Student's *t*-tests. **H** Pathogenicity assay of WT, *VdNuo1* mutants, and complemented strains on shantung maple. Shantung maple seedlings were inoculated with indicated strains, while the H_2O treatment served as a negative control. The Verticillium wilt symptoms were photographed at 35 dpi. Ten 1-month-old plants were inoculated one time, and the experiment was replicated three times. The pathogen was re-isolated from treated seedlings on V8 medium after incubation for 4 days in the dark at 25 °C. **I** Quantification of the fungal biomass in maple stems by qPCR following inoculation of the indicated strains. Samples were collected from the stem base of infected seedlings at 35 dpi. The *At18S* gene of shantung maple was used as an endogenous control to evaluate the colonization of *V. dahliae* by quantifying *VdEF-1a*. The fungal biomass was calculated from three independent biological replicates. Error bars represent standard errors of the mean. $^{***}P < 0.001$ is the probability associated with the one-way ANOVA

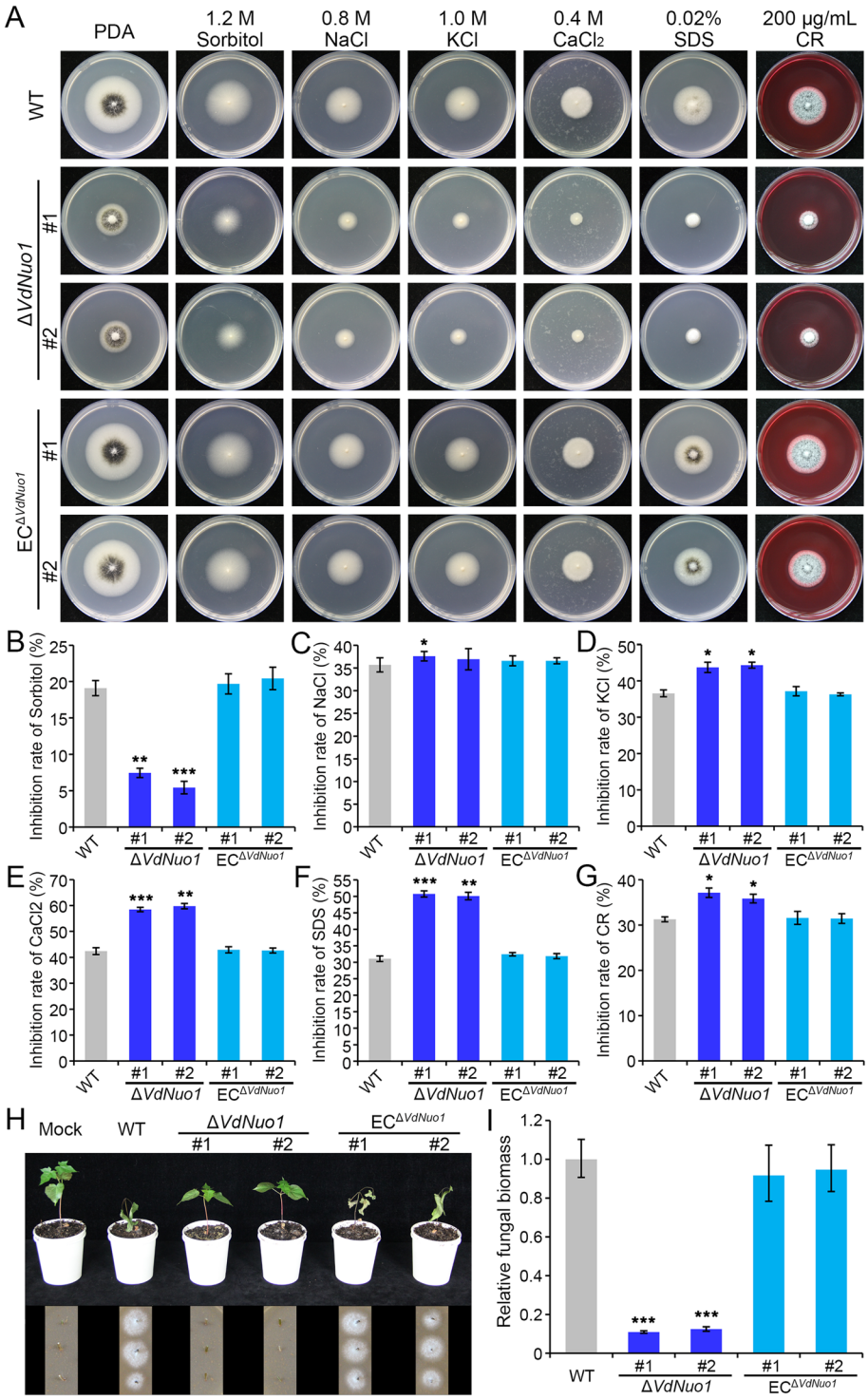

Fig. 5 (See legend on previous page.)

Given the mitochondrial localization of VdNuo1 and the changed transcriptomic profile in mutants, the morphology of mitochondria was observed by transmission electron microscopy. In the WT and complemented strains, the mitochondria were intact and their cristae were clear (Fig. S6B). However, the deletion of *VdNuo1* led to the formation of giant lipid droplets, dispersion of outer mitochondrial membrane, and the fusion of the

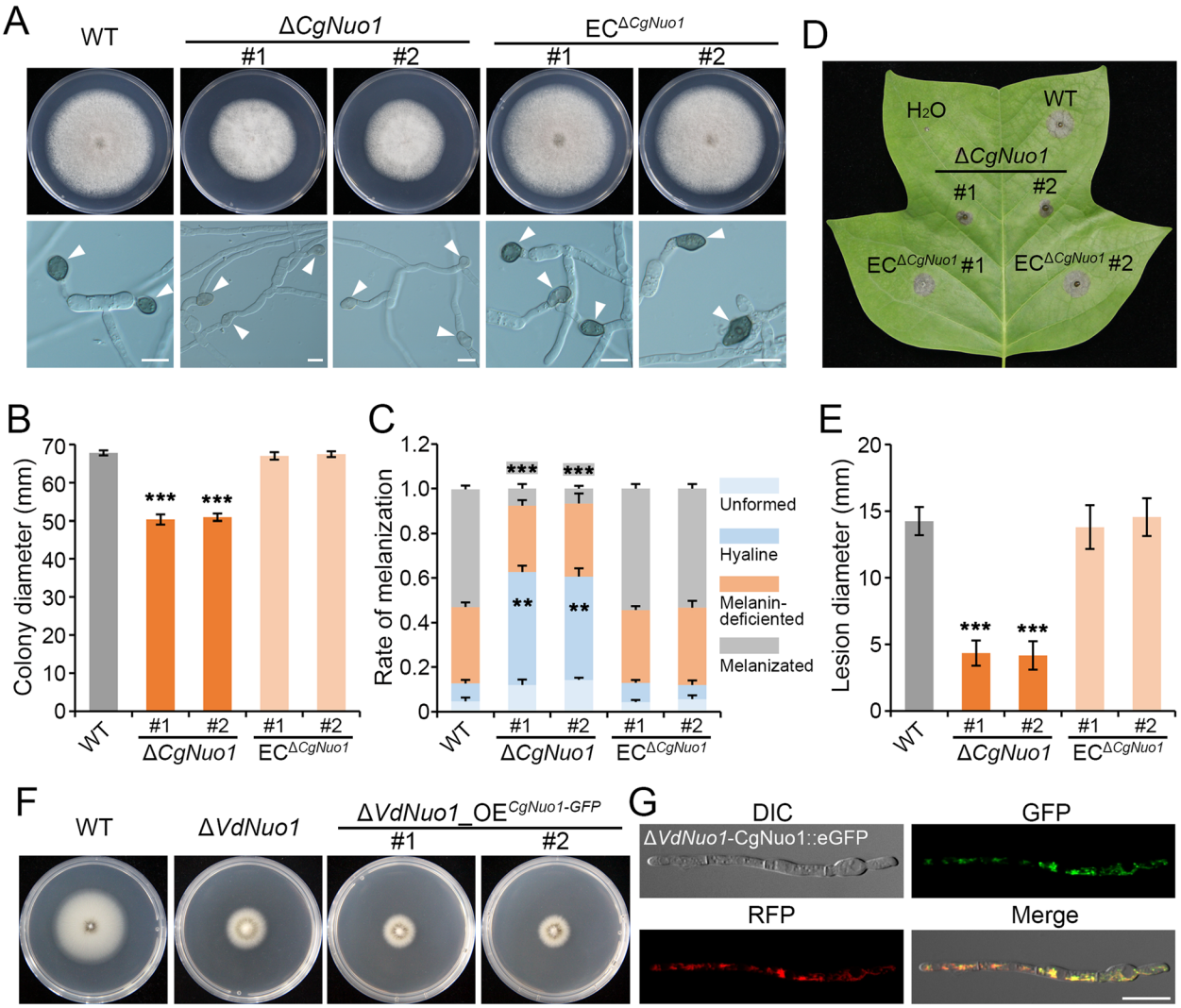

Fig. 6 *Nuo1* homologues of *Verticillium dahliae* and *Colletotrichum gloeosporioides* are functionally conserved, but incompatible in heterologous expression analysis. **A** Colony morphology and appressoria of WT, *CgNuo1* mutants, and complemented strains. The strains were grown on PDA plates in the dark at 25 °C for 5 days. Each strain was inoculated on at least three plates and three independent experiments were carried out. The conidia of each strain were incubated on hydrophobic glass slides for 12 h to observe the appressoria melanization (arrows). For each strain, 120 appressoria were observed, and the experiment was replicated three times. **B** and **C** Colony diameter and appressoria number of the indicated strains in **A**. Error bars are standard errors calculated from six colony diameters (**B**), $^{***}P < 0.001$ (Student's *t*-test). The appressoria were divided into four levels, and the hyaline and melanized appressoria were counted (**C**). Error bars represent standard errors. $^{**}P < 0.01$, $^{***}P < 0.001$ (Student's *t*-test). These experiments were replicated three times. **D** and **E** Pathogenicity assay of the indicated strains on *L. chinense*. The conidial suspensions of each strain were inoculated on one leaf after being punctured at 25 °C in the dark for 4 days (**D**). The diameters were calculated from the lesions of each strain on six leaves (**E**). Error bars represent standard errors. $^{***}P < 0.001$ (Student's *t*-test). This experiment was repeated 3 times, with 6 leaves inoculated in each experiment. **F** Colony morphology of *CgNuo1* heterologous expression strains. The GFP-fused recombinant plasmid was transferred in *VdNuo1* mutants. The positive transformants, *VdNuo1* mutant, and WT strain grown on PDA plates in the dark at 25 °C for 7 days. Each strain was inoculated at least three plates and three independent experiments were carried out. **G** The fluorescence signal observation of *CgNuo1* heterologous expression strains. The indicated positive transformants in **F** were incubated on hydrophobic glass slides in a dark at 25 °C for 16 h. The germinating hyphae were stained by the mitochondrial probe (CMXRos), then the GFP and RFP signals were observed by fluorescence microscopy. Scale bar = 10 μm

matrix with cristae (Fig. S6B). These results suggested that VdNuo1 mediates aspects of morphological integrity of mitochondria. To identify VdNuo1 as a potential control target, mtROS inducers (menadione) and several fungicides, including melanin inhibitor (tricyclazole), ergosterol inhibitors (terbinafine and voriconazole), and pleiotropic fungicides (tubermycin B), were tested. The significantly increased sensitivity of the mutant to

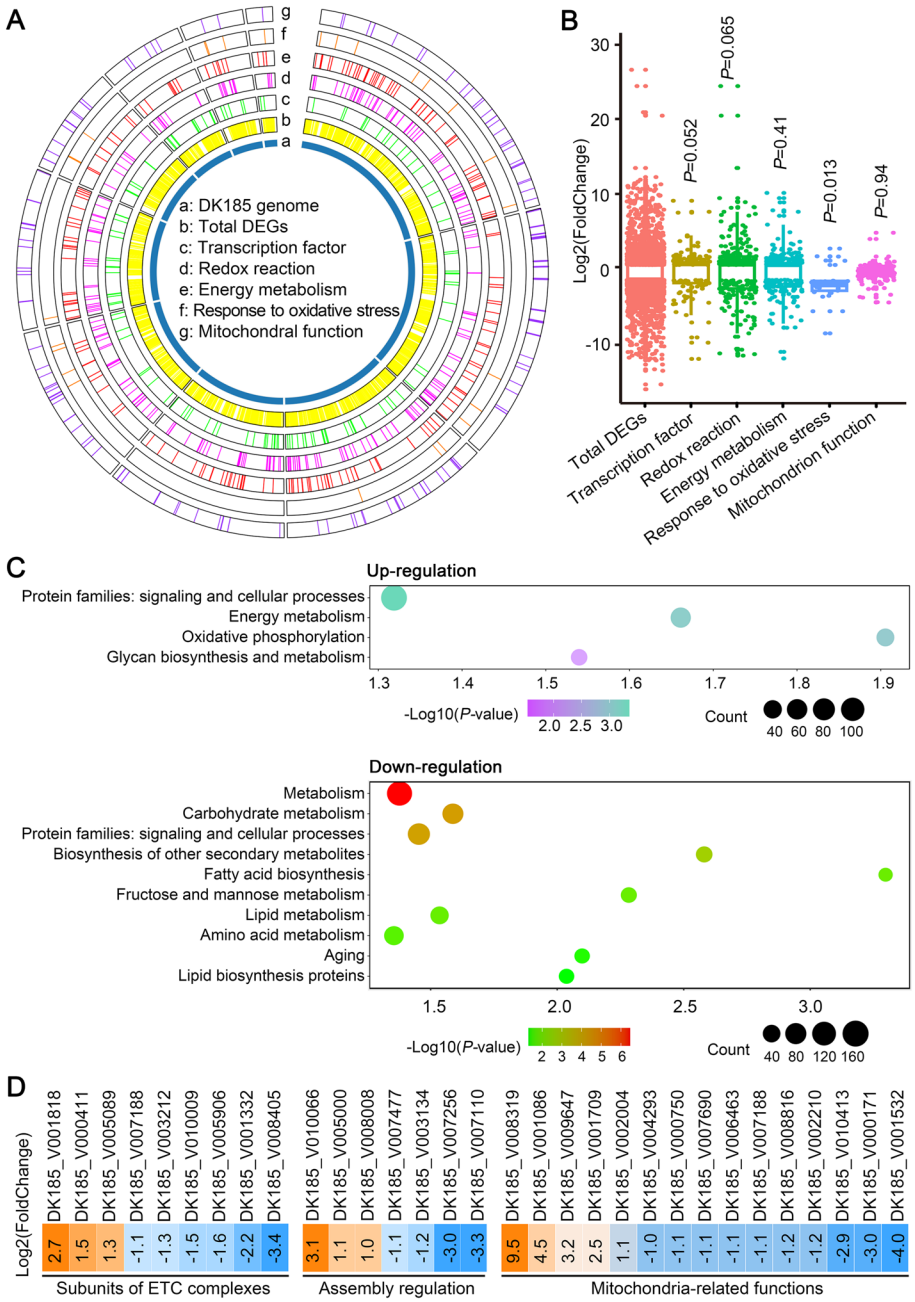

Fig. 7 RNA-seq analysis reveals altered transcription in the *VdNou1* deletion mutant of *Verticillium dahliae*. **A** Transcriptome comparison of *VdNou1* deletion mutant compared with the WT strain. Distribution of differentially expressed genes (DEGs) among gene ontology terms of transcription factors, redox reaction, energy metabolism, response to oxidative stress, and mitochondrial process in *V. dahliae* DK185 genome. The DEGs of *VdNou1* deletion mutant versus WT with cutoff log2 ratio ≥ 2 and *P* value < 0.01. **B** Fold change range of DEGs regulated by *VdNou1*. The significance is calculated by the values of log2(fold change) in transcription factors, redox reaction, energy metabolism, responses to oxidative stress, and mitochondrial process-related DEGs compared with total DEGs. The *P* values are from two-tailed Wilcoxon rank sum test. **C** KEGG enrichment analyses between wild-type and *VdNou1* deletion mutant of *V. dahliae*. KEGG enrichment analysis was performed using TBtools with *P* value < 0.05. **D** Heat map for the transcriptional expression of respiratory chain complex-related genes, including complex subunits, complex assembly regulatory components, and mitochondria-related genes. The fold change is the value of the log2 ratio; the corresponding gene ID (AT13 strain) is at the top of the colored blocks

menadione indicated that VdNuo1 contributes to mitochondrial superoxide anion detoxification (Fig. S6B and C). Overall, these results suggested that mitochondria-related effects of *VdNuo1* are multifunctional and global in *V. dahliae*.

Discussion

The transmembrane complex I is conserved among mammals, plants, and fungi and serves as an entry for electrons from NADH into the ETC [9, 18]. So far, homologous subunits of complex I have been identified and investigated in many species [3, 21, 27, 28]. However, the functions of complex I in fungi, especially in filamentous fungi, have not been fully explored. Herein, we identified the complex I 24-kDa subunit (VdNuo1) in *V. dahliae* and verified its subcellular localization, carried out three-dimensional structure prediction, and examined its phylogeny (Fig. 1). VdNuo1 is important for mitochondrial morphogenesis and mediates vegetative growth, metabolism, melanin biosynthesis, microsclerotia development, stress tolerance, and virulence in *V. dahliae*. We further confirmed that at least one of its homologues shares similar functions but the results suggest that these are relatively independent in plant pathogenic fungi. Moreover, comparative transcriptome analysis of the WT and *VdNuo1* deletion strain provides a blueprint to analyze the global role of *VdNuo1* in *V. dahliae.* The multiple physiological and pathological functions indicate that it is an excellent site for controlling the pathogen.

Among the 42 subunits of fungal mitochondrial complex I, the 24-kDa and 51-kDa subunits are coupled and spatially located at the entrance of the redox centers (N module) [3, 9]. Although the 24-kDa subunit may be dispensable in electron transport, it plays a critical role in the assembly and enzyme activity of complex I [21, 47, 56]. The loss of *VdNuo1* in *V. dahliae* deprives NADH: ubiquinone oxidoreductase activity and ultimately exhibits resistance to rotenone (Fig. 2A and B). The differential response of mutants to inhibitors (Fig. 2A, C, and D) suggests that *VdNuo1* has a systematic impact on the mitochondrial respiratory chain. Dysfunction of complex II and III can disrupt histone methylation and mtROS levels, respectively [6, 8, 57, 58]. These respiratory chain defects are consistent with mitochondrial morphological phenotypes (Fig. S6B). As the first step in the ETC, the integrity of complex I is essential for mitochondrial metabolism. In fungi and mammals, the ATP deficiency caused by ECT disruption can be compensated by gluconeogenesis or negatively regulating fatty acid transport and β-oxidation [27, 59]. The RNA-seq results showed that expression levels of genes (DK185_V008205, DK185_V000141, DK185_V001371, DK185_V008341, DK185_V007731, DK185_V008392, DK185_V000812, and others) associated with gluconeogenesis and fatty acid biosynthesis in *VdNuo1* mutants were disordered compared with the WT (supplementary Table S4). These findings may further explain disruption of mitochondrial sugar and fatty acid metabolism in *VdNuo1* mutants (Fig. S2A–E). In addition, the formation of large lipid droplets (Fig. S6B) may be attributed to the accumulation of polyunsaturated fatty acids. The content of unsaturated fatty acids affects the fluidity and permeability of the membrane [60, 61]. The imbalance of unsaturated fatty acids (Fig. S2F) may also be a response to ROS to reduce cell damage caused by lipid peroxidation.

Dysfunction of the respiratory chain complex I impairs cell development in almost all organisms. For fungi, several complex I subunits have reported to be involved in sporulation, sexual reproduction, and vegetative growth [26, 27, 62]. These predictable defects emerged in *VdNuo1* mutants, such as delayed growth and decreased conidiation (Fig. 3A–G). This is supported by the RNA-seq results, which showed disturbances in energy metabolism, mitochondrial activity, and synthesis of various cellular components (Figs. 7 and S6). In *V. dahliae*, defective polar growth leads to decreased hyphal growth [63, 64]. In this study, *VdNuo1* mutants did not display defective polar growth as assessed by chitin staining and conidial germination (Fig. 3I). The expression of *VdNuo1* throughout the life cycle of *V. dahliae*, but particularly at the time of microsclerotia production (Fig. 3H), suggests that *VdNuo1* plays a role in a unique developmental phase, during the formation and melanization of microsclerotia.

The 1,8-dihydroxynaphthalene melanin (DHN melanin) is ubiquitous in the microbial kingdom with a kaleidoscope of functions [54]. In this study, we observed that the 24-kDa subunit VdNuo1 positively regulates melanin biosynthesis (Figs. 4A–E, 6C and E). In *V. dahliae*, the metabolic regulation and function of melanin are obscure. Melanin production is tightly coupled to microsclerotia formation, hyphal growth, and resistance to various stresses [37, 41, 43, 53, 63], but its production is not required for pathogenicity [36]. Although *VdNuo1* mutants did not affect penetration (Fig. 4F), they were more sensitive to high ion concentrations and cell wall stresses, which may be partially attributed to insufficient melanin biosynthesis (Fig. 5A and C–G). Moreover, the sensitivity to ion may also be related to changes in mitochondrial IMM permeability, stress, and calcium homeostasis caused by complex I functional disorders [65]. Few studies have revealed the relationship between complex I and virulence [25, 28, 66]. Obviously, the absence of 24-kDa Nuo1 subunits significantly reduces the pathogenicity of both in *V. dahliae* and *C. gloeosporioides* (Figs. 5H, I, 6D, E, and S4). Indeed, the reduced

pathogenicity of *C. gloeosporioides* is most likely due to insufficient melanization in appressoria. Since there is no direct evidence to suggest that melanin is a pathogenicity factor in *V. dahliae* [36, 67], the reduced pathogenicity is most likely due to the multiple pleiotropic effects on metabolism, though increasing studies indicate crosstalk between melanin biosynthesis and other signaling pathways that regulate pathogenicity [37, 40–42]. Thus, further research on *VdNuo1* will provide new insights into the correlation between the lack of melanin production and pathogenesis in *V. dahliae*.

The *VdNuo1* homologue in *C. gloeosporioides* also showed functional conservation in vegetative growth (Fig. 6A and B). Meanwhile, *CgNuo1* was expressed in *V. dahliae* and localized in mitochondria but could not recover the growth phenotype (Fig. 6F and G). This incompatibility could be explained by multiple factors. First, different species are subjected to different evolutionary selection pressures, and thus the two orthologous subunits are not clustered on the same evolutionary branch (Fig. 1F). Second, phylogenetic analysis of mitochondrial genome has placed *V. dahliae* in the *Verticillium* spp. lineage [16]. Mitochondria may have functions in species-specific niche adaptation, infection, and morphogenesis of *V. dahliae*. The deficiency of complex I enzyme activity may be corrected by transfection with homologues, while the majority of subunits are acquired independently along various evolutionary lineages [20, 68] that define the uniqueness of each subunit in each species. Moreover, variable tRNA abundances lead to codon usage bias among species. Ribosome elongation efficiency and protein stability depend on this [69]. Thus, the optimization of codons between *V. dahliae* and *C. gloeosporioides* should also be considered.

Currently, the overuse of antibiotics has led to the evolution of drug-resistant microbes, posing significant challenges to food safety, and human and plant health. Targets within fungal mitochondria hold an untapped potential for the development of fungicides owing to the fact that their protein composition and enzyme activity differs from those of mammals and plants [8, 18, 70]. Mitochondrial morphogenesis mediated by VdNuo1 (Fig. S6B) is fundamental to multiple biological functions and the global transcriptional regulation in *V. dahliae*. Tests of fungicides (Fig. S6C and D) suggest that disrupting mitochondrial superoxide anion metabolism may be an effective strategy to control *V. dahliae*. The role of VdNuo1 in this process remains to be explored further.

Conclusions

In conclusion, we identified the 24-kDa subunit VdNuo1 associated with mitochondrial development that is important for growth, metabolism, mitochondrial homeostasis, microsclerotia development, resistance to stress, and virulence in *V. dahliae*. Furthermore, the conserved mitochondrial localization and functions of homologues suggest that Nuo1 may provide an effective target for precise control of Verticillium wilt and other phytopathogenic fungi.

Methods

Fungal strains and growth conditions

The wild-type *V. dahliae* strain AT13 was isolated from infected shantung maple [71]. The homologues were cloned from *C. gloeosporioides* strain SMCG1#C, the anthracnose pathogen of *Cunninghamia lanceolata* and *L. chinensis*×*tulipifera* [72], was previously stored in a laboratory.

The WT, mutants, and (heterologous) complemented *V. dahliae* and *C. gloeosporioides* strains in this study were stored at − 80 °C in 25% glycerin and were cultured on PDA (200 g potato, 20 g glucose, and 15 g agar per liter) medium at 25 °C in the dark. Resistant strains were screened on medium supplemented with hygromycin (50 μg/mL) and/or geneticin (50 μg/mL) (500 μg/mL for *C. gloeosporioides* mutants). All strains were shaken in liquid complete medium (CM, 6 g yeast extract, 6 g acid-hydrolyzed casein, 10 g sucrose per liter) about 2 days at 25 °C for collecting conidia.

The ATMT (*Agrobacterium tumefaciens* mediated-transformation) method and medium (MM and IM) were described by Maruthachalam et al. [73]. Colony phenotypes of vegetative growth, stress or inhibitor tolerance, carbon source, or fatty acid utilization were analyzed on PDA and Czapek (2 g $NaNO_3$, 1 g K_2HPO_4, 0.5 g KCl, 0.5 g $MgSO_4$, 0.01 g $FeSO_4$, 30 g sucrose, 15 g agar and add water to 1 L; sucrose was replaced by 17 g starch, 10 g pectin, and 10 g sodium carboxymethyl cellulose, respectively) medium at 25 °C in the dark for 7 days.

The development of microsclerotia was examined following incubation on BMM medium (5 g glucose, 0.2 g $NaNO_3$, 0.52 g KCl, 0.52 g $MgSO_4{\cdot}7H_2O$, 1.52 g KH_2PO_4, 3 μM vitamin B1, 0.1 mM vitamin H, 15 g agar, with the pH adjusted to 7.5 and water added to 1 L). The MM medium was also used to permeation assays.

Characterization and phylogenetic analysis

The analyses of the FeS cluster and the NuoE motif were conducted using online bioinformatics analysis tools such as InterPro (http://www.ebi.ac.uk/interpro/), Pfam (http://pfam.xfam.org/), and SMART (http://smart.embl-heidelberg.de/), with the threshold e value $< 10^{-5}$. The mitochondrial presequences were predicted by MitoFates (https://mitf.cbrc.pj.aist.go.jp/MitoFates), then these domains were presented by IBS (Illustrator for Biological

Sequences). The three-dimensional protein structure was predicted and drawn by SWISS-MODEL (https://www.expasy.org/resources/swiss-model). The homologues in fungi were identified using the National Center for Biological Information (NCBI) database (https://www.ncbi.nlm.nih.gov/). Based on the protein sequences of homologues, the phylogenetic tree was constructed using MEGA 7.0 with the NJ algorithm (http://www.megasoftware.net/).

Gene deletions, mutant complementation, and heterologous expression

To obtain deletion mutants and complemented strains, genomic DNA was extracted using a DNA isolation kit (Vazyme, Nanjing, China). The RNA required in this study was extracted and reverse transcribed by the kits (Aidlab Biotech, Beijing, China; TransGen Biotech, Beijing, China). All steps followed the manufacturer's instructions.

The 5′- and 3′-flanking regions (0.8–1.5 kb) of the target genes were amplified with specific primers listed in supplementary Table S1 and the flanks were inserted in a hygromycin resistance gene cassette (*hyg*) in plasmid pDHt2 [74]. The plasmid was linearized by endonuclease *EcoR*I and *Xba*I, and the flanks were incorporated by homologous recombination using a Clon Express II One Step Cloning Kit (Vazyme, Nanjing, China). Similarly, the fragments including the native promoters (0.8–1.2 kb) and terminators (0.5–0.8 kb) of the target genes were fused with a *Xba*I/*EcoR*I-digested pCOM vector [74] containing the geneticin resistance cassette (*G418*) to construct the complementary vector. To generate the plasmid for heterologous expression, the CDS (coding sequence) of homologous gene was amplified from cDNA of *C. gloeosporioides* and inserted into an *Xba*I/*Sac*I-digested pCOM-T0161 vector (pCOM vector added with TrpC promoter). The recombinant plasmids were transferred into *Agrobacterium tumefaciens* strain AGL-1 to carry out the ATMT [73] in the corresponding strains. The positive transformants were identified by antibiotic resistance evaluation and the transformations were confirmed by multiple diagnostic PCR with specific primers listed in supplementary Table S1.

Subcellular localization and chitin staining

To generate the GFP-fusion strains, the CDS regions of *VdNuo1* and *CgNuo1* without stop codons and GFP fragment were amplified and inserted into a *Xba*I/*Sac*I-digested pCOM-T0161 vector by homologous recombination. The sequenced recombinant plasmids were transferred to the WT and *VdNuo1* deletion strains by ATMT. The specific primer pairs related to the above experiments are listed in supplementary Table S1. Before single-spore purification, resistant transformants were detected by GFP signal observation using a Carl Zeiss Imager.M2 light microscopy system.

To observe fluorescence and chitin distribution, the conidial suspensions of each strain were collected and diluted into 10^4 spores/mL. Each conidial suspension (10 μL) was incubated on hydrophobic glass slides in the dark at 25 °C. After 16 h, preheated 200 nM mitochondrial probe (Mito-Tracker Red CMXRos, Beyotime Biotechnology, Shanghai, China) and 20 μg/mL CFW (Sigma, USA) were used for staining followed by a rinse. The fluorescence signals were observed using GFP (excitation wavelength (Ex) 470 nm, emission wavelength (Em) 525 nm), RFP (Ex 545 nm, Em 605 nm), and DAPI (Ex 365 nm, Em 445 nm) channels. The fluorescence intensity was determined by ImageJ.

The samples (conidia) of mitochondrial morphology were collected from Czapek plates and observed by transmission electron microscopy (HITACHI HT7800, Japan) at 80 kV voltage and in HC mode. Before slicing (Leica EM UC7, Germany) and staining (uranyl acetate and lead citrate), samples were pre-washed (0.2 M phosphate buffer and 1% osmium tetroxide), fixed (2.5% glutaraldehyde), dehydrated (30% to 100% ethanol), infiltrated (1:2, 1:1 and pure resin), and polymerized.

Evaluation of morphology, tolerance, penetration, and microsclerotia formation

All strains were grown on PDA at 25 °C in the dark for 5 days. The hyphal blocks were cut from the edge of each colony and were inoculated on corresponding plates for observation of growth and inhibition phenotypes, penetration, and microsclerotia development. All the reagents used were purchased from Solarbio (Beijing Solarbio Science and Technology). Each experiment was repeated three times independently.

To investigate the growth and resistance of *V. dahliae* to respiratory chain inhibitors, fungicides, and other stressors, each strain was cultured on Czapek (salt) or PDA medium supplied with carbon sources (sugars and plant cell wall components), respiratory chain (complex I, II, and III) inhibitors, fungicides (terbinafine, voriconazole, tricyclazole, tubermycin B, and menadione), and abiotic factors (high-osmosis, cation, and cell wall integrity stress). All these treatments were cultured in the dark at 25 °C for 7 days. The colony cross diameters were measured to characterize vegetative growth. The inhibition rates were obtained from the formula: 100% × (control diameter − treatment group diameter)/control diameter. The effect of sugar on each strain was calculated by 100% × treatment group diameter/control diameter.

In simulated penetration experiments, each strain was incubated on MM medium covered with cellophane

membranes (Beijing Solarbio Science and Technology) at 25 °C in the dark. The membranes were removed at 72 hpi, and the strains were grown for another 5 days. Five replicates of each medium were inoculated per experiment.

To measure the conidiation of each strain, five 0.5 mm diameter hyphal plugs were collected with a hole puncher from the edge of the colonies that were grown on PDA medium for 7 days, and then shaken in sterile water containing 0.1% Tween-20 for 1 min. Conidia were counted using a hemocytometer, with three repeats for each strain. Subsequently, the conidia were used to perform germination experiments. Before observation of hyphae and appressoria morphology, the conidial suspensions of each strain were diluted to 10^4 spores/mL and incubated on hydrophobic glass slides in the dark at 25 °C for 16 (hyphae) or 12 h (appressoria). The germination and melanization rate of 120 appressoria were tested.

Microsclerotia induction was examined using methods of a previous study [37]. Briefly, the diluted conidial suspensions (3×10^6/mL) of each strain were coated (20 μL) on BMM medium covered by cellophane membranes at 25 °C in the dark. The morphology of microsclerotia was observed under a stereomicroscope at 5, 7, and 14 dpi. Each strain was inoculated on five plates. The number, size, and melanization ratio were calculated from 60 fields (0.25 mm^2), 150 diameters, and 30 pictures (gray value calculated by ImageJ) of the microsclerotia.

Analysis of fatty acid composition and RNA-seq

The analysis of fatty acid composition of the samples was conducted by Suzhou PANOMIX Biomedical Tech Co., LTD. Prior to this analysis, all strains were grown on Czapek medium covered with cellophane membranes at 25 °C in the dark for 5 days. Fifty milligrams of hyphae was ground with liquid nitrogen and was ultrasonically extracted with 1 mL chloroform methanol solution (2: 1, V/V). After centrifugation, the supernatant was shaken with 2 mL of 1% methanol sulfate solution, and esterification at 80 °C for 30 min. The esterified products were extracted with 1 mL n-hexane and centrifuged. Twenty microliters of dehydrated supernatant was diluted with n-hexane to 400 μL. Finally, 20 μL methyl salicylate (500-ppm) was supplemented as internal standard for GC–MS/MS (Trace 1310-ISQ 7000, USA). GC condition: Thermo TG-FAME (50 m*0.25 mm ID*0.20 μm); injection volume: 1 μL; oven temperature program started at 80 °C, held for 1 min, and was raised (1) with a rate of 20 °C min^{-1} to 160 °C, held for 1.5 min; (2) with a rate of 3 °C min^{-1} to 196 °C, held for 8.5 min; and (3) with a rate of 20 °C min^{-1} to 250 °C, held for 3 min. Helium was used as the carrier gas with a column flow of 0.63 mL min^{-1}. The MS condition included an electron impact ionization mode (70 eV) with selected ion monitoring (SIM). The contents of each fatty acid are shown in supplementary Table S3.

The sample preparation, sequencing, and data analysis followed methods from a previous study [37]. In brief, samples of the WT and *VdNuo1* mutants of *V. dahliae* for RNA extraction were cultured on Czapek medium for 5 days. Illumina HiSeq XTen was used to construct and sequence the library. The detailed statistics for the RNA-seq are listed in supplementary Table S4, including the raw read numbers, clean reads, RNA RIN scores, and mapping rates. Raw data were filtered to obtain clean reads through SOAPnuke with the parameters as -l 15 -q 0.2 -n 0.1 -Q 2 (https://github.com/-flexlab/SOAPnuke). The clean reads were mapped to the *V. dahliae* strain AT13 (DK185) genome using the HISAT2 (v0.1.6-bata) [75]. The RSEM (v1.2.12) was used to quantify the expression of genes and transcripts to obtain FPKM values [76]. DEseq2 was performed to detect the differential genes with the parameters of fold change ≥ 2.00 and an adjusted *P* value of ≤ 0.05. For the RNA-seq analysis, differentially expressed genes (DEGs, in supplementary Table S4) from three biological replicates of the mutant and WT were identified by Deseq R with a false discovery rate of 1% (fold change ≥ 2.0, $P < 0.01$). Based on the value of fold change in the expression of genes, the DEGs were analyzed using gene ontology (GO) analysis and Kyoto Encyclopedia of Genes and Genomes (KEGG) analysis, including biological process, molecular function, cellular component, and various metabolic and response pathways. The threshold for the significant enrichment of GO terms was $P < 0.05$.

Pathogenicity and colonization assay

The cotton (Junmian No.1) and shantung maple seedlings were grown 3–4 weeks in a greenhouse at 25 °C. The conidial suspensions of each strain were collected and diluted. The inoculation of the pathogen was accomplished using a root-dip inoculation method [36]. Seedlings were removed from the soil medium, then the washed roots were immersed in the conidial suspensions (5×10^6 for cotton and 5×10^7 spores/mL for maple) for 30 min. Twenty cotton or 10 maple seedlings were inoculated with each strain. This experiment was repeated independently for 3 times with water treated seedlings as negative controls. Based on the progression of disease in different hosts, we observed the Verticillium wilt symptoms and collected cotton and maple samples for fungal biomass analyses and reisolation at 21 and 35 dpi. Subsequently, the stems of cottons were longitudinally dissected to observe vascular discoloration, while the inoculated stems near the rachis of each maple seedling were cut and placed on V8 medium (200 mL V8

vegetable juice, 2 g $CaCO_3$, and 15 g agar per liter) to reisolate the pathogens.

For the pathogenicity assays with *C. gloeosporioides*, conidial suspensions (1×10^6 spores/mL) of each strain were obtained by overnight shaking in PDB medium at 25 °C. The leaves of *L. chinensis*×*tulipifera* that were collected from the Nanjing Forestry University were washed and inoculated after being stabbed with a needle. All strains were inoculated on one leaf at 25 °C in a dark for 4 days. This experiment was repeated three times, with 6 leaves inoculated in each experiment.

Analysis of relative gene expression and fungal biomass

To detect the expression profile of *VdNuo1* during the life cycle, 20 μL of WT strain conidial suspension of 5×10^6 spores/mL was coated on the cellophane membrane covered on the BMM medium. The samples were collected at 2, 3, 4, 5, 7, 10, and 14 dpi described in previous study [41], and the conidia were used as control. Similarly, the relative expression levels of melanin-related genes in each strain were detected in the samples collected on the 7th day of microsclerotia observation. The fungal biomass samples of cottons and maples were collected after pathogenicity assays at 21 and 35 dpi, respectively. These samples were stored at − 80 °C until use. The samples required for validation of RNA-seq results refer to sequencing sample preparation.

Total RNA (gene expression samples) and DNA (fungal biomass samples) were extracted; the RNA was further reverse-transcribed into cDNA. In the fungal biomass analysis, qPCR (quantitative PCR) was carried out with the cotton and maple 18S rDNA gene (*Gh18S* and *At18S*) as internal reference genes to quantify DNA of *V. dahliae* using the target of elongation factor 1α gene *VdEF-1α*. For analyses relative gene expression, the *VdEF-1α* of *V. dahliae* was used as normalization to quantify the expression of related genes by reverse transcription-quantitative PCR (RT-qPCR).

The amplification reactions were carried out using 2×Top Green qPCR SuperMix (TransGen Biotech, Beijing, China) and the QuantStudio3 Real-Time PCR system (Thermo Fisher Scientific, USA). The reaction volumes of both RT-qPCR and qPCR included 20 μL (10 μL SuperMix, 1.2 μL primer pair, 1.5 μL cDNA or gDNA, and 7.3 μL ddH_2O). The reaction procedures included pre-denaturation at 95 °C for 3 min, followed by 40 cycles of 95 °C denaturation for 15 s, 60 °C annealing for 20 s, and 72 °C extension for 20 s (signal collection), followed by a termination step. There were three replicates for each qPCR and RT-qPCR experiment, enabling calculations of mean and standard error. The $2^{-\Delta\Delta CT}$ method [77] was used to calculate the relative expression levels or pathogen biomass contents. Each assay was independently repeated 3 times to ensure the consistency of results. The primer pairs of genes related to this experiment were listed in supplementary Table S2. The cDNA was used in a five-step tenfold dilution standard curve (50 ng to 5 pg) to test the amplification efficiency of primer pairs. All assays were between 90 and 100% efficient.

Statistical analysis

All experiments were conducted independently 3 times, and each contained at least 3 biological replicates. The mean ± SD was calculated from data obtained from these replicates, which included 3 replicates for expression or biomass levels, 6 for colony diameters, 150 for microsclerotia diameters, and microsclerotia number and melanin coverage in 60 and 30 visual fields, respectively. These calculations were performed only after the assumptions of normality and equal variance were met. Significant differences in the colony or lesion diameter, conidiation, appressoria development, and inhibition rate of each treatment, as well as the numbers, size, and gray value of microsclerotia, were analyzed by an ordinary Student's *t*-test using Microsoft Excel. Moreover, significant differences of gene expression levels and fungal biomass were identified using one-way analysis of variance (ANOVA) followed by mean separation test using least significant difference to determine treatment differences, while the effect of sugar on each strain was analyzed by multivariate analysis of variance (MANOVA). Statistical analyses were performed using the SPSS version 19 software package (SPSS Inc., Chicago, IL, USA).

Abbreviations

ATP	Adenosine triphosphate
ETC	Electron transport chain
IMM	Inner mitochondrial membrane
mtROS	Mitochondrial reactive oxygen species
MALCs	Mono-alkyl lipophilic cations
GFP	Green fluorescent protein
aa	Amino acids
FeS	Iron-sulfur
PDA	Potato dextrose agar
WT	Wilt type
EC	Ectopic complemented transformants
OE	Overexpressed strain
CMC-Na	Sodium carboxymethyl cellulose
BMM	Modified basal agar medium
dpi/hpi	Days/hours post inoculation
CFW	Calcofluor White
MM	Minimal
SDS	Sodium dodecyl sulfate
CR	Congo red
RNA-seq	RNA sequencing
GO	Gene ontology
DEGs	Differentially expressed genes
KEGG	Kyoto Encyclopedia of Genes and Genomes
ATMT	*Agrobacterium tumefaciens* Mediated-transformation
hyg	Hygromycin resistance gene cassette
G418	Geneticin resistance cassette
CDS	Coding sequence
qPCR/RT-qPCR	Quantitative PCR/reverse transcription-quantitative PCR

Supplementary Information

The online version contains supplementary material available at https://doi.org/10.1186/s12915-024-02084-9.

Additional file 1: Supplementary figures. Fig. S1 Diagnostic PCR of VdNuo1 mutants and complement strains. Fig. S2 Sugar and fatty acid metabolic functions of VdNuo1. Fig. S3 Observation of VdNuo1-mediared microsclerotia development at 7 dpi. Fig. S4 Pathogenicity assays of VdNuo1 on cotton. Fig. S5 Diagnostic PCR of CgNuo1 mutants, complement strains, and heterologous expression strains. Fig. S6 Quantitative detection of RNA-seq results

Additional file 2: Supplementary tables. Table S1 Information on the primer pairs used to construct the vector in this study. Table S2 Information of RT-qPCR primer pairs used in this study. Table S3 Quantitative analysis of fatty acid components in WT and VdNuo1 mutant. Table S4 Data quality and refined DEGs of RNA-seq analysis

Additional file 3: Raw data

Acknowledgements
We thank Prof. Lin Huang of Nanjing Forestry University for providing *C. gloeosporioides* strain.

Authors' contributions
FMC, DDZ, ZQK, KVS and JYC conceived and designed the experiments. HL and YL performed main experiments, including mutant construction, plate phenotype, morphological observation, pathogenicity evaluation, gene expression analysis, and homologous gene identification. HL and DW was responsible for transcriptomic analysis. YHW and RCS participated in constructing VdNuo1 mutants and mitochondrial staining. HL and DW analyzed the data. HL, DDZ and FMC wrote the initial draft. KVS, JYC and SJK reviewed and edited the manuscript. FMC, JYC and HL provided the funding for this research. All authors read and approved the final manuscript. The authors declare no competing financial interests.

Funding
This work was supported by the National Natural Science Foundation of Jiangsu province (BK2024655), the China Postdoctoral Science Foundation (2023M731706), the National Key Research and Development Program of China (2022YFE0130800), the National Natural Science Foundation of China (32071768, 32370213, 32302327), the Agricultural Sciences Talent Program CAAS (J.Y.C.), and the Agricultural Science and Technology Innovation Program grant (J.Y.C.).

Data availability
All data generated or analyzed during this study are included in the article, its supplementary information files are publicly available in repositories. The RNA-seq data presented in this study were conducted in one project and respectively, deposited in the NCBI Sequence Read Archive (SRA) database under project accession number PRJNA835225 (WT strain, previous study) [37] and PRJNA1130377 (VdNuo1 mutant, this study).

Declarations

Ethics approval and consent to participate
This article does not contain any experiments with animals or human participants that were performed by the contributing authors.

Consent for publication
Not applicable.

Competing interests
The authors declare no competing interests.

Author details
[1]Co-Innovation Center for Sustainable Forestry in Southern China, Nanjing Forestry University, Nanjing 210037, Jiangsu, China. [2]State Key Laboratory for Biology of Plant Diseases and Insect Pests, Institute of Plant Protection, Chinese Academy of Agricultural Sciences, Beijing 100193, China. [3]Western Agricultural Research Center, Chinese Academy of Agricultural Sciences, Changji 831100, China. [4]State Key Laboratory of Subtropical Silviculture, School of Forestry and Biotechnology, Zhejiang A & F University, Hangzhou 311300, China. [5]United States Department of Agriculture, Agricultural Research Service, Sam Farr United States Crop Improvement and Protection Research Center, Salinas, CA, USA. [6]Department of Plant Pathology, University of California, Davis, c/o Sam Farr United States Crop Improvement and Protection Research Center, University of California, Davis, Salinas, CA, USA.

Received: 20 August 2024 Accepted: 29 November 2024
Published online: 18 December 2024

References

1. Spinelli JB, Haigis MC. The multifaceted contributions of mitochondria to cellular metabolism. Nat Cell Biol. 2018;20(7):745–54. https://doi.org/10.1038/s41556-018-0124-1.
2. Averbeck D, Rodriguez-Lafrasse C. Role of mitochondria in radiation responses: epigenetic, metabolic, and signaling impacts. Int J Mol Sci. 2021;22(20):11047. https://doi.org/10.3390/ijms222011047.
3. Vercellino I, Sazanov LA. The assembly, regulation and function of the mitochondrial respiratory chain. Nat Rev Mol Cell Biol. 2022;23(2):141–61. https://doi.org/10.1038/s41580-021-00415-0.
4. Guo X, Aviles G, Liu Y, Tian R, Unger BA, Lin YT, Wiita AP, Xu K, Correia MA, Kampmann M. Mitochondrial stress is relayed to the cytosol by an OMA1-DELE1-HRI pathway. Nature. 2020;579(7799):427–32. https://doi.org/10.1038/s41586-020-2078-2.
5. Zhu D, Li X, Tian Y. Mitochondrial-to-nuclear communication in aging: an epigenetic perspective. Trends Biochem Sci. 2022;47(8):645–59. https://doi.org/10.1016/j.tibs.2022.03.008.
6. Zhu J, Schwörer S, Berisa M, Kyung YJ, Ryu KW, Yi J, Jiang X, Cross JR, Thompson CB. Mitochondrial NADP(H) generation is essential for proline biosynthesis. Science. 2021;372(6545):968–72. https://doi.org/10.1126/science.abd5491.
7. Lucas JA, Hawkins NJ, Fraaije BA. The evolution of fungicide resistance. Adv Appl Microbiol. 2015;90:29–92. https://doi.org/10.1016/bs.aambs.2014.09.001.
8. Steinberg G, Schuster M, Gurr SJ, Schrader TA, Schrader M, Wood M, Early A, Kilaru S. A lipophilic cation protects crops against fungal pathogens by multiple modes of action. Nat Commun. 2020;11(1):1608. https://doi.org/10.1038/s41467-020-14949-y.
9. Vinothkumar KR, Zhu J, Hirst J. Architecture of mammalian respiratory complex I. Nature. 2014;515(7525):80–4. https://doi.org/10.1038/nature13686.
10. Meyer EH, Welchen E, Carrie C. Assembly of the complexes of the oxidative phosphorylation system in land plant mitochondria. Annu Rev Plant Biol. 2019;70:23–50. https://doi.org/10.1146/annurev-arplant-050718-100412.
11. Jones AJY, Blaza JN, Varghese F, Hirst J. Respiratory complex I in *Bos taurus* and *Paracoccus denitrificans* pumps four protons across the membrane for every NADH oxidized. J Biol Chem. 2017;292(12):4987–95. https://doi.org/10.1074/jbc.M116.771899.
12. Protasoni M, Pérez-Pérez R, Lobo-Jarne T, Harbour ME, Ding S, Peñas A, Diaz F, Moraes CT, Fearnley IM, Zeviani M, Ugalde C, Fernández-Vizarra E. Respiratory supercomplexes act as a platform for complex III-mediated maturation of human mitochondrial complexes I and IV. EMBO J. 2020;39(3):e102817. https://doi.org/10.15252/embj.2019102817.
13. Haws SA, Leech CM, Denu JM. Metabolism and the epigenome: a dynamic relationship. Trends Biochem Sci. 2020;45(9):731–47. https://doi.org/10.1016/j.tibs.2020.04.002.
14. Lautrup S, Sinclair DA, Mattson MP, Fang EF. NAD^+ in brain aging and neurodegenerative disorders. Cell Metab. 2019;30(4):630–55. https://doi.org/10.1016/j.cmet.2019.09.001.
15. Redza-Dutordoir M, Averill-Bates DA. Activation of apoptosis signalling pathways by reactive oxygen species. Biochim Biophys Acta. 2016;1863(12):2977–92. https://doi.org/10.1016/j.bbamcr.2016.09.012.
16. Jelen V, de Jonge R, Van de Peer Y, Javornik B, Jakše J. Complete mitochondrial genome of the Verticillium-wilt causing plant pathogen

Verticillium nonalfalfae. PLoS ONE. 2016;11(2): e0148525. https://doi.org/10.1371/journal.pone.0148525.
17. Roger AJ, Muñoz-Gómez SA, Kamikawa R. The origin and diversification of mitochondria. Curr Biol. 2017;27(21):R1177–92. https://doi.org/10.1016/j.cub.2017.09.015.
18. Wang G, Wang Y, Ni J, Li R, Zhu F, Wang R, Tian Q, Shen Q, Yang Q, Tang J, Murcha MW, Wang G. An MCIA-like complex is required for mitochondrial complex I assembly and seed development in maize. Mol Plant. 2022;15(9):1470–87. https://doi.org/10.1016/j.molp.2022.08.001.
19. Klusch N, Senkler J, Yildiz Ö, Kühlbrandt W, Braun HP. A ferredoxin bridge connects the two arms of plant mitochondrial complex I. Plant Cell. 2021;33:2072–91. https://doi.org/10.1093/plcell/koab092.
20. Elurbe DM, Huynen MA. The origin of the supernumerary subunits and assembly factors of complex I: a treasure trove of pathway evolution. Biochim Biophys Acta. 2016;1857(7):971–9. https://doi.org/10.1016/j.bbabio.2016.03.027.
21. Zickermann V, Zwicker K, Tocilescu MA, Kerscher S, Brandt U. Characterization of a subcomplex of mitochondrial NADH: ubiquinone oxidoreductase (complex I) lacking the flavoprotein part of the N-module. Biochim Biophys Acta. 2007;1767(5):393–400. https://doi.org/10.1016/j.bbabio.2007.03.005.
22. Sazanov LA. A giant molecular proton pump: structure and mechanism of respiratory complex I. Nat Rev Mol Cell Biol. 2015;16(6):375–88. https://doi.org/10.1038/nrm3997.
23. Ghezzi D, Zeviani M. Human diseases associated with defects in assembly of OXPHOS complexes. Essays Biochem. 2018;62(3):271–86. https://doi.org/10.1042/EBC20170099.
24. González-Rodríguez P, Zampese E, Stout KA, Guzman JN, Ilijic E, Yang B, Tkatch T, Stavarache MA, Wokosin DL, Gao L, Kaplitt MG, López-Barneo J, Schumacker PT, Surmeier DJ. Disruption of mitochondrial complex I induces progressive parkinsonism. Nature. 2021;599(7886):650–6. https://doi.org/10.1038/s41586-021-04059-0.
25. She X, Khamooshi K, Gao Y, Shen Y, Lv Y, Calderone R, Fonzi W, Liu W, Li D. Fungal-specific subunits of the *Candida albicans* mitochondrial complex I drive diverse cell functions including cell wall synthesis. Cell Microbiol. 2015;17(9):1350–64. https://doi.org/10.1111/cmi.12438.
26. Zhao H, Wang Q, Liu C, Shang Y, Wen F, Wang F, Liu W, Xiao W, Li W. A role for the respiratory chain in regulating meiosis initiation in *Saccharomyces cerevisiae*. Genetics. 2018;208(3):1181–94. https://doi.org/10.1534/genetics.118.300689.
27. Cai X, Zhang S, Lin J, Wang Y, Ye F, Zhou B, Lin Q, Liu J. Role of the gene ndufs8 located in respiratory complex I from *Monascus purpureus* in the cell growth and secondary metabolites biosynthesis. J Fungi (Basel). 2022;8(7):655. https://doi.org/10.3390/jof8070655.
28. Huang X, Chen X, He Y, Yu X, Li S, Gao N, Niu L, Mao Y, Wang Y, Wu X, Wu W, Wu J, Zhou D, Zhan X, Chen C. Mitochondrial complex I bridges a connection between regulation of carbon flexibility and gastrointestinal commensalism in the human fungal pathogen *Candida albicans*. PLoS Pathog. 2017;13(6): e1006414. https://doi.org/10.1371/journal.ppat.1006414.
29. Galkin A, Brandt U. Superoxide radical formation by pure complex I (NADH: ubiquinone oxidoreductase) from *Yarrowia lipolytica*. J Biol Chem. 2005;280(34):30129–35. https://doi.org/10.1074/jbc.M504709200.
30. Carneiro P, Duarte M, Videira A. Disruption of alternative NAD(P)H dehydrogenases leads to decreased mitochondrial ROS in *Neurospora crassa*. Free Radic Biol Med. 2012;52(2):402–9. https://doi.org/10.1016/j.freeradbiomed.2011.10.492.
31. Kretschmer M, Klose J, Kronstad JW. Defects in mitochondrial and peroxisomal β-oxidation influence virulence in the maize pathogen *Ustilago maydis*. Eukaryot Cell. 2012;11(8):1055–66. https://doi.org/10.1128/EC.00129-12.
32. Verma S, Shakya VPS, Idnurm A. Exploring and exploiting the connection between mitochondria and the virulence of human pathogenic fungi. Virulence. 2018;9(1):426–46. https://doi.org/10.1080/21505594.2017.1414133.
33. Klosterman SJ, Subbarao KV, Kang S, Veronese P, Gold SE, Thomma BP, Chen Z, Henrissat B, Lee YH, Park J, Garcia-Pedrajas MD, Barbara DJ, Anchieta A, de Jonge R, Santhanam P, Maruthachalam K, Atallah Z, Amyotte SG, Paz Z, Inderbitzin P, Hayes RJ, Heiman DI, Young S, Zeng Q, Engels R, Galagan J, Cuomo CA, Dobinson KF, Ma LJ. Comparative genomics yields insights into niche adaptation of plant vascular wilt pathogens. PLoS Pathog. 2011;7(7): e1002137. https://doi.org/10.1371/journal.ppat.1002137.
34. Klimes A, Dobinson KF, Thomma BP, Klosterman SJ. Genomics spurs rapid advances in our understanding of the biology of vascular wilt pathogens in the genus *Verticillium*. Annu Rev Phytopathol. 2015;2015(53):181–98. https://doi.org/10.1146/annurev-phyto-080614-120224.
35. Chen JY, Klosterman SJ, Hu XP, Dai XF, Subbarao KV. Key insights and research prospects at the dawn of the population genomics era for *Verticillium dahliae*. Annu Rev Phytopathol. 2021;59:31–51. https://doi.org/10.1146/annurev-phyto-020620-121925.
36. Wang Y, Hu X, Fang Y, Anchieta A, Goldman PH, Hernandez G, Klosterman SJ. Transcription factor VdCmr1 is required for pigment production, protection from UV irradiation, and regulates expression of melanin biosynthetic genes in *Verticillium dahliae*. Microbiology (Reading). 2018;164(4):685–96. https://doi.org/10.1099/mic.0.000633.
37. Li H, Wang D, Zhang DD, Geng Q, Li JJ, Sheng RC, Xue HS, Zhu H, Kong ZQ, Dai XF, Klosterman SJ, Subbarao KV, Chen FM, Chen JY. A polyketide synthase from *Verticillium dahliae* modulates melanin biosynthesis and hyphal growth to promote virulence. BMC Biol. 2022;20(1):125. https://doi.org/10.1186/s12915-022-01330-2.
38. Zhang DD, Dai XF, Klosterman SJ, Subbarao KV, Chen JY. The secretome of *Verticillium dahliae* in collusion with plant defence responses modulates Verticillium wilt symptoms. Biol Rev Camb Philos Soc. 2022;97(5):1810–22. https://doi.org/10.1111/brv.12863.
39. Reusche M, Truskina J, Thole K, Nagel L, Rindfleisch S, Tran VT, Braus-Stromeyer SA, Braus GH, Teichmann T, Lipka V. Infections with the vascular pathogens *Verticillium longisporum* and *Verticillium dahliae* induce distinct disease symptoms and differentially affect drought stress tolerance of *Arabidopsis thaliana*. Environ Exp Bot. 2014;108:23–37. https://doi.org/10.1016/j.envexpbot.2013.12.009.
40. Luo X, Mao H, Wei Y, Cai J, Xie C, Sui A, Yang X, Dong J. The fungal-specific transcription factor Vdpf influences conidia production, melanized microsclerotia formation and pathogenicity in *Verticillium dahliae*. Mol Plant Pathol. 2016;17(9):1364–81. https://doi.org/10.1111/mpp.12367.
41. Wang Y, Tian L, Xiong D, Klosterman SJ, Xiao S, Tian C. The mitogen-activated protein kinase gene, VdHog1, regulates osmotic stress response, microsclerotia formation and virulence in *Verticillium dahliae*. Fungal Genet Biol. 2016;88:13–23. https://doi.org/10.1016/j.fgb.2016.01.011.
42. Tang C, Jin X, Klosterman SJ, Wang Y. Convergent and distinctive functions of transcription factors VdYap1, VdAtf1, and VdSkn7 in the regulation of nitrosative stress resistance, microsclerotia formation, and virulence in *Verticillium dahliae*. Mol Plant Pathol. 2020;21(11):1451–66. https://doi.org/10.1111/mpp.12988.
43. Li H, Sheng RC, Zhang CN, Wang LC, Li M, Wang YH, Qiao YH, Klosterman SJ, Chen JY, Kong ZQ, Subbarao KV, Chen FM, Zhang DD. Two zinc finger proteins, VdZFP1 and VdZFP2, interact with VdCmr1 to promote melanized microsclerotia development and stress tolerance in *Verticillium dahliae*. BMC Biol. 2023;21(1):237. https://doi.org/10.1186/s12915-023-01697-w.
44. Wu XM, Zhang BS, Zhao YL, Wu HW, Gao F, Zhang J, Zhao JH, Guo HS. DeSUMOylation of a *Verticillium dahliae* enolase facilitates virulence by derepressing the expression of the effector VdSCP8. Nat Commun. 2023;14(1):4844. https://doi.org/10.1038/s41467-023-40384-w.
45. Su X, Rehman L, Guo H, Li X, Zhang R, Cheng H. AAC as a potential target gene to control *Verticillium dahliae*. Genes (Basel). 2017;8(1):25. https://doi.org/10.3390/genes8010025.
46. Zeng H, Li T, Tian J, Zhang LL. TUBP1 protein lead to mitochondria-mediated apoptotic cell death in *Verticillium dahliae*. Int J Biochem Cell Biol. 2018;103:35–44. https://doi.org/10.1016/j.biocel.2018.08.001.
47. Almeida T, Duarte M, Melo AM, Videira A. The 24-kDa iron-sulphur subunit of complex I is required for enzyme activity. Eur J Biochem. 1999;265(1):86–93. https://doi.org/10.1046/j.1432-1327.1999.00668.x.
48. Duan Y, Lu F, Zhou Z, Zhao H, Zhang J, Mao Y, Li M, Wang J, Zhou M. Quinone outside inhibitors affect DON biosynthesis, mitochondrial structure and toxisome formation in *Fusarium graminearum*. J Hazard Mater. 2020;398:122908. https://doi.org/10.1016/j.jhazmat.2020.122908.
49. Li S, Li X, Zhang H, Wang Z, Xu H. The research progress in and perspective of potential fungicides: succinate dehydrogenase inhibitors. Bioorg Med Chem. 2021;50: 116476. https://doi.org/10.1016/j.bmc.2021.116476.
50. Liu S, Ruan W, Li J, Xu H, Wang J, Gao Y, Wang J. Biological control of phytopathogenic fungi by fatty acids. Mycopathologia. 2008;166(2):93–102. https://doi.org/10.1007/s11046-008-9124-1.

51. Wu S, Zhang Q, Zhang W, Huang W, Kong Q, Liu Q, Li W, Zou X, Liu CM, Yan S. Linolenic acid-derived oxylipins inhibit aflatoxin biosynthesis in *Aspergillus flavus* through activation of imizoquin biosynthesis. J Agric Food Chem. 2022;70(50):15928–44. https://doi.org/10.1021/acs.jafc.2c06230.
52. Duressa D, Anchieta A, Chen D, Klimes A, Garcia-Pedrajas MD, Dobinson KF, Klosterman SJ. RNA-seq analyses of gene expression in the microsclerotia of *Verticillium dahliae*. BMC Genomics. 2013;14:607. https://doi.org/10.1186/1471-2164-14-607.
53. Li JJ, Zhou L, Yin CM, Zhang DD, Klosterman SJ, Wang BL, Song J, Wang D, Hu XP, Subbarao KV, Chen JY, Dai XF. The *Verticillium dahliae* Sho1-MAPK pathway regulates melanin biosynthesis and is required for cotton infection. Environ Microbiol. 2019;21(12):4852–74. https://doi.org/10.1111/1462-2920.14846.
54. Kogej T, Wheeler MH, Rizner TL, Gunde-Cimerman N. Evidence for 1,8-dihydroxynaphthalene melanin in three halophilic black yeasts grown under saline and non-saline conditions. FEMS Microbiol Lett. 2004;232(2):203–9. https://doi.org/10.1016/S0378-1097(04)00073-4.
55. Lopez-Moya F, Martin-Urdiroz M, Oses-Ruiz M, Were VM, Fricker MD, Littlejohn G, Lopez-Llorca LV, Talbot NJ. Chitosan inhibits septin-mediated plant infection by the rice blast fungus *Magnaporthe oryzae* in a protein kinase C and Nox1 NADPH oxidase-dependent manner. New Phytol. 2021;230(4):1578–93. https://doi.org/10.1111/nph.17268.
56. Zu Y, Di Bernardo S, Yagi T, Hirst J. Redox properties of the [2Fe-2S] center in the 24 kDa (NQO2) subunit of NADH: ubiquinone oxidoreductase (complex I). Biochemistry. 2002;41(31):10056–69. https://doi.org/10.1021/bi026026f.
57. Zhao RZ, Jiang S, Zhang L, Yu ZB. Mitochondrial electron transport chain, ROS generation and uncoupling (review). Int J Mol Med. 2019;44(1):3–15. https://doi.org/10.3892/ijmm.2019.4188.
58. Mangalhara KC, Varanasi SK, Johnson MA, Burns MJ, Rojas GR, Esparza Moltó PB, Sainz AG, Tadepalle N, Abbott KL, Mendiratta G, Chen D, Farsakoglu Y, Kunchok T, Hoffmann FA, Parisi B, Rincon M, Vander Heiden MG, Bosenberg M, Hargreaves DC, Kaech SM, Shadel GS. Manipulating mitochondrial electron flow enhances tumor immunogenicity. Science. 2023;381(6664):1316–23. https://doi.org/10.1126/science.abq1053.
59. Enkler L, Szentgyörgyi V, Pennauer M, Prescianotto-Baschong C, Riezman I, Wiesyk A, Avraham RE, Spiess M, Zalckvar E, Kucharczyk R, Riezman H, Spang A. Arf1 coordinates fatty acid metabolism and mitochondrial homeostasis. Nat Cell Biol. 2023;25(8):1157–72. https://doi.org/10.1038/s41556-023-01180-2.
60. Waldhart AN, Muhire B, Johnson B, Pettinga D, Madaj ZB, Wolfrum E, Dykstra H, Wegert V, Pospisilik JA, Han X, Wu N. Excess dietary carbohydrate affects mitochondrial integrity as observed in brown adipose tissue. Cell Rep. 2021;36(5): 109488. https://doi.org/10.1016/j.celrep.2021.109488.
61. Menezes LB, Segat BB, Tolentino H, Pires DC, Mattos LMM, Hottum HM, Pereira MD, Latini A, Horn A Jr, Fernandes C. ROS scavenging of SOD/CAT mimics probed by EPR and reduction of lipid peroxidation in *S. cerevisiae* and mouse liver, under severe hydroxyl radical stress condition. J Inorg Biochem. 2023;239:112062. https://doi.org/10.1016/j.jinorgbio.2022.112062.
62. Duarte M, Videira A. Respiratory chain complex I is essential for sexual development in neurospora and binding of iron sulfur clusters are required for enzyme assembly. Genetics. 2000;156(2):607–15. https://doi.org/10.1093/genetics/156.2.607.
63. Xiong D, Wang Y, Tian L, Tian C. MADS-box transcription factor VdMcm1 regulates conidiation, microsclerotia formation, pathogenicity, and secondary metabolism of *Verticillium dahliae*. Front Microbiol. 2016;7:1192. https://doi.org/10.3389/fmicb.2016.01192.
64. Tian L, Yu J, Wang Y, Tian C. The C_2H_2 transcription factor VdMsn2 controls hyphal growth, microsclerotia formation, and virulence of *Verticillium dahliae*. Fungal Biol. 2017;121(12):1001–10. https://doi.org/10.1016/j.funbio.2017.08.005.
65. Steffen W, Gemperli AC, Cvetesic N, Steuber J. Organelle-specific expression of subunit ND5 of human complex I (NADH dehydrogenase) alters cation homeostasis in *Saccharomyces cerevisiae*. FEMS Yeast Res. 2010;10(6):648–59. https://doi.org/10.1111/j.1567-1364.2010.00643.x.
66. Bromley M, Johns A, Davies E, Fraczek M, Mabey Gilsenan J, Kurbatova N, Keays M, Kapushesky M, Gut M, Gut I, Denning DW, Bowyer P. Mitochondrial complex I is a global regulator of secondary metabolism, virulence and azole sensitivity in fungi. PLoS ONE. 2016;11(7): e0158724. https://doi.org/10.1371/journal.pone.0158724.
67. Sarmiento-Villamil JL, García-Pedrajas NE, Baeza-Montañez L, García-Pedrajas MD. The APSES transcription factor Vst1 is a key regulator of development in microsclerotium- and resting mycelium-producing Verticillium species. Mol Plant Pathol. 2018;19(1):59–76. https://doi.org/10.1111/mpp.12496.
68. Bai Y, Hájek P, Chomyn A, Chan E, Seo BB, Matsuno-Yagi A, Yagi T, Attardi G. Lack of complex I activity in human cells carrying a mutation in MtDNA-encoded ND4 subunit is corrected by the *Saccharomyces cerevisiae* NADH-quinone oxidoreductase (NDI1) gene. J Biol Chem. 2001;276(42):38808–13. https://doi.org/10.1074/jbc.M106363200.
69. Bae H, Coller J. Codon optimality-mediated mRNA degradation: linking translational elongation to mRNA stability. Mol Cell. 2022;82(8):1467–76. https://doi.org/10.1016/j.molcel.2022.03.032.
70. Wirth C, Brandt U, Hunte C, Zickermann V. Structure and function of mitochondrial complex I. Biochim Biophys Acta. 2016;1857(7):902–14. https://doi.org/10.1016/j.bbabio.2016.02.013.
71. Li H, Zhou LF, Wang LC, Zhao XH, Chen FM. Wilt of shantung maple caused by *Verticillium dahliae* in China. Plant Disease. 2017;102(1). https://doi.org/10.1094/PDIS-07-17-1037-PDN.
72. Wang P, Li B, Pan YT, Zhang YZ, Li DW, Huang L. Calcineurin-responsive transcription factor CgCrzA is required for cell wall integrity and infection-related morphogenesis in *Colletotrichum gloeosporioides*. Plant Pathol J. 2020;36(5):385–97. https://doi.org/10.5423/ppj.oa.04.2020.0071.
73. Maruthachalam K, Klosterman SJ, Kang S, Hayes RJ, Subbarao KV. Identification of pathogenicity-related genes in the vascular wilt fungus *Verticillium dahliae* by Agrobacterium tumefaciens-mediated T-DNA insertional mutagenesis. Mol Biotechnol. 2011;49(3):209–21. https://doi.org/10.1007/s12033-011-9392-8.
74. Zhou L, Zhao J, Guo W, Zhang T. Functional analysis of autophagy genes via Agrobacterium-mediated transformation in the vascular wilt fungus *Verticillium dahliae*. J Genet Genomics. 2013;40(8):421–31. https://doi.org/10.1016/j.jgg.2013.04.006.
75. Kim D, Langmead B, Salzberg SL. HISAT: a fast spliced aligner with low memory requirements. Nat Methods. 2015;12(4):357–60. https://doi.org/10.1038/nmeth.3317.
76. Li B, Dewey CN. RSEM: accurate transcript quantification from RNA-seq data with or without a reference genome. BMC Bioinformatics. 2011;12:323. https://doi.org/10.1186/1471-2105-12-323.
77. Livak KJ, Schmittgen TD. Analysis of relative gene expression data using real-time quantitative PCR and the 2(-delta delta C(T)) method. Methods. 2001;25(4):402–8. https://doi.org/10.1006/meth.2001.1262.

Publisher's Note